Title

A multi-channel electrophysiology approach to non-invasively and precisely record human spinal cord activity

Authors

Birgit Nierula[1,+], Tilman Stephani[2,3,4,#], Emma Bailey[1], Merve Kaptan[1,4], Lisa-Marie Pohle[1], Ulrike Horn[1], André Mouraux[5], Burkhard Maess[6], Arno Villringer[3], Gabriel Curio[7], Vadim V. Nikulin[2,3,7†], Falk Eippert[1†*]

Affiliations

[1] Max Planck Research Group Pain Perception, Max Planck Institute for Human Cognitive and Brain Sciences, 04103 Leipzig, Germany.
[2] Research Group Neural Interactions and Dynamics, Department of Neurology, Max Planck Institute for Human Cognitive and Brain Sciences, 04103 Leipzig, Germany.
[3] Department of Neurology, Max Planck Institute for Human Cognitive and Brain Sciences, 04103 Leipzig, Germany.
[4] International Max Planck Research School NeuroCom, 04103 Leipzig, Germany.
[5] Institute of Neuroscience, Université Catholique de Louvain, 1200 Brussels, Belgium.
[6] Methods and Development Group Brain Networks, Max Planck Institute for Human Cognitive and Brain Sciences, 04103 Leipzig, Germany.
[7] Department of Neurology, Charité University Medicine, 12200 Berlin, Germany.
+ Now at Fraunhofer Heinrich-Hertz-Institute, Department for Vision and Imaging Technology, Interactive and Cognitive Systems Group, Berlin, Germany.
# Now at Radboud University, Donders Institute for Brain, Cognition and Behaviour, Nijmegen, The Netherlands
† These authors contributed equally to this work.

* Corresponding author address: Falk Eippert, Max Planck Institute for Human Cognitive and Brain Sciences, Stephanstraße 1a, 04103 Leipzig, Germany; eippert@cbs.mpg.de.

Author contributions

Author contributions listed alphabetically according to CRediT taxonomy (https://credit.niso.org):
Conceptualization: FE, BN, VVN.
Data curation: BN.
Formal analysis: EB, MK, BN, LMP, TS.
Funding acquisition: FE.
Investigation: LMP, BN.
Methodology: EB, GC, FE, UH, AM, BN, VVN, LMP.
Project administration: FE, BN.
Resources: FE, VVN, AV.
Software: EB, MK, BN, TS.
Supervision: FE, VVN.
Visualization: BN, FE.
Writing – original draft: FE, BN.
Writing – review & editing: EB, GC, FE, MK, UH, BM, AM, BN, VVN, LMP, TS, AV.

Abstract

The spinal cord is of fundamental importance for integrative processing in brain-body communication, yet routine non-invasive recordings in humans are hindered by vast methodological challenges. Here we overcome these challenges by developing an easy-to-use electrophysiological approach based on high-density multi-channel spinal recordings combined with multivariate spatial-filtering analyses. These advances enable a spatiotemporal characterization of spinal cord responses and demonstrate a sensitivity that permits assessing even single-trial responses. To furthermore enable the study of integrative processing along the neural processing hierarchy in somatosensation, we expand this approach by simultaneous peripheral, spinal and cortical recordings and provide direct evidence that bottom-up integrative processing occurs already within the spinal cord and thus after the first synaptic relay in the central nervous system. Finally, we demonstrate the versatility of this approach by providing non-invasive recordings of nociceptive spinal cord responses during heat-pain stimulation. Beyond establishing a new window on human spinal cord function at millisecond timescale, this work provides the foundation to study brain-body communication in its entirety in health and disease.

Introduction

The spinal cord is an important interface for reciprocal brain-body communication in sensory, motor and autonomic domains [1]. Traditionally, it has been portrayed as a relay station, yet recent studies challenge this long-held view, for example in the somatosensory domain, where a high degree of neuronal complexity and circuit organization has been delineated in animal models, suggestive of extensive integrative processing [2–4]. Such advances are important in order to arrive at a mechanistic understanding of spinal processing, especially considering the spinal cord's central role in numerous neurological disorders [5–7] as well as in treatment approaches for spinal cord injury [8,9] or biomarker development for analgesic drug discovery [10,11]. While there is a continuous development of sophisticated spinal recording technologies in experimental animals [12,13], such progress is missing in human neuroscience and knowledge on processing in the human spinal cord is consequently very limited, thus presenting a missing link in a comprehensive understanding of brain-body communication in health and disease.

Approaches such as reflex recordings [14,15] allow for useful assessments of the processes occurring within the human spinal cord, yet they only provide an indirect picture and more direct assessments via neuroimaging techniques are highly desirable. Several factors make the spinal cord a very challenging target for non-invasive neuroimaging however: it has a small diameter, is located deep in the body in close proximity to inner organs such as the heart and lungs, and is protected by the vertebral column and muscle layers. Consequently, there is a lack of well-established and readily-available approaches to interrogate human spinal cord function. For example, functional magnetic resonance imaging (fMRI) of the human spinal cord [16] comes with major technical challenges [17] and is fundamentally limited by its indirect link to neuronal activity via neurovascular coupling and ensuing low temporal resolution. Magnetospinography (MSG) on the other hand is a non-invasive method that directly measures the magnetic fields generated by neuronal populations in the spinal cord with high temporal precision [18], yet no commercially available systems have been developed [19]. Both approaches are therefore only pursued by a small number of research groups and additionally require major investments in large-scale equipment, preventing their widespread use in human neuroscience.

Here, we introduce a novel approach that overcomes these issues. It is based on an enhancement of methodology established several decades ago during the development of non-invasive electrospinography (ESG) [20–24]. These studies recorded somatosensory evoked potentials (SEPs) from the human spinal cord via surface electrodes placed on the skin over the vertebral column and reported SEPs with a post-synaptic origin in the dorsal horn of the spinal cord [25–30]. While useful in clinical settings [31,32], due to technical challenges this line of research has however largely subsided in experimental neuroscience, with only a handful of studies recording such spinal SEPs non-invasively in healthy human volunteers in the last decade [33–38].

To improve upon these approaches and expand the insights ESG can offer, we leveraged the developments that have occurred in recording capabilities and processing techniques for neurophysiological data [39–41]: we developed a non-invasive approach that allows for recording spinal signals with high temporal precision (10 kHz) as well as extensive spatial coverage (multi-channel montage of 39 surface electrodes placed over the neck and trunk in two dense electrode grids) and combined this with concurrent recordings of the input to (peripheral nerve action potentials, NAPs) and output from the spinal cord (brainstem and cortical SEPs). Furthermore, we developed dedicated artifact-correction techniques to enhance the spinal signal-to-noise ratio and employed multivariate analysis approaches that allowed for increased robustness as well as extraction of spinal cord responses at single-trial level.

This approach thus provides a direct and easily-accessible electrophysiological window into a previously missing link of brain-body communication relevant for several domains in human

neuroscience. Here, we chose the domain of somatosensation as test-bed and employed this approach in two complementary studies (Figure 1), in both of which we recorded signals from the cervical and lumbar spinal cord, in order to allow for the generalization of our findings across upper and lower limb representations. Most importantly, this approach allowed us to directly investigate whether integrative processes already occur at the level of the human spinal cord, i.e. at the first station of central nervous system processing. In a final proof-of-principle experiment, we furthermore assess the possibility of using this non-invasive approach to detect nociceptive spinal cord responses in humans.

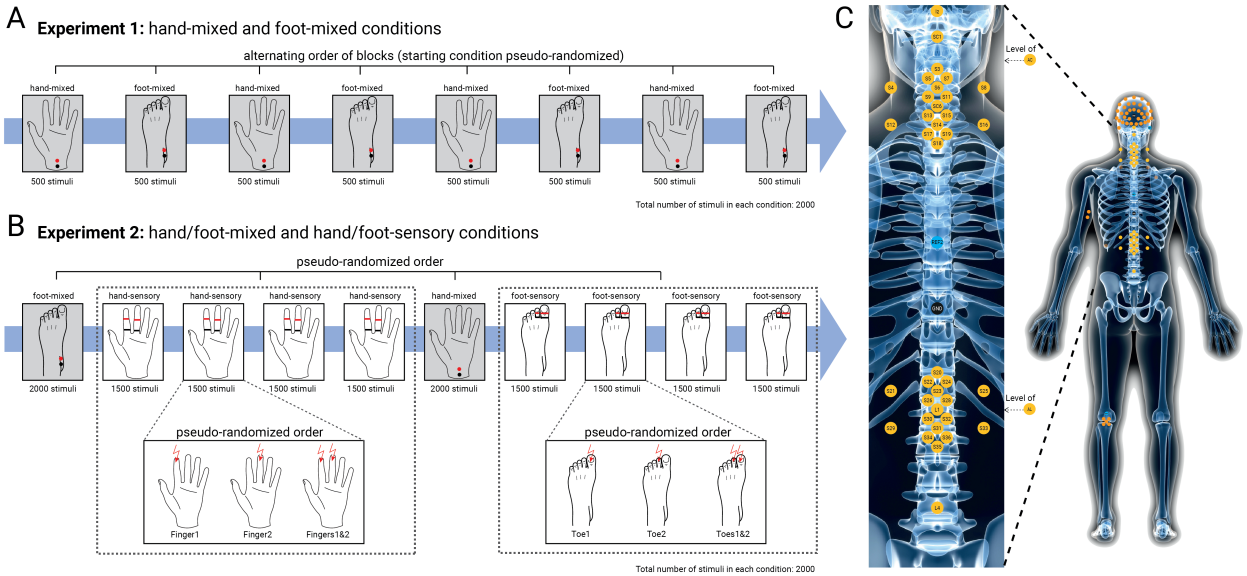

***Figure 1. Overview of experimental conditions and recording setup**. **A)** In Experiment 1, electrical mixed nerve stimulation was applied to the left median nerve at the wrist (hand-mixed) and to the left tibial nerve at the ankle (foot-mixed). Four hand-mixed and four foot-mixed blocks were presented in alternating order. **B)** In Experiment 2, electrical mixed nerve stimulation was applied to the same location as in Experiment 1 and electrical sensory nerve stimulation was applied to the left index and middle finger (hand-sensory) and to the first and second toe (foot-sensory). Sensory stimulation blocks were separated into 4 consecutive blocks of the same stimulation type (either hand-sensory or foot-sensory). **C)** Across both experiments, responses were recorded at the level of the peripheral nerves, the spinal cord, and the brain. Peripheral NAPs were recorded from the ipsilateral axilla and Erb's point for median nerve stimulation and from the ipsilateral popliteal fossa (cluster of 5 electrodes) and the cauda equina for tibial nerve stimulation. Spinal cord SEPs were recorded with a montage of 37 dorsal and 2 ventral electrodes, which had a cervical and a lumbar focus: around an anatomical target electrode (placed over the spinous process of either the 6th cervical vertebra or the 1st lumbar vertebra), 17 electrodes were placed in a grid with distances optimized for capturing the spatial distribution of the spinal signal. Additionally, the following electrodes were contained in the spinal montage: one over the inion, one over the first cervical vertebra, one over the spinous process of the 4th lumbar vertebra, and two ventral electrodes (AC located supra-glottically and AL located supra-umbilically). All electrodes of the spinal montage were referenced to an electrode placed over the spinous process of the 6th thoracic vertebra. Cortical SEPs were recorded with a 64-channel EEG setup in Experiment 1 (39 channels in Experiment 2).*

Results

Delineating somatosensory responses along the neural hierarchy (Experiment 1)

As a first objective, we aimed to replicate previously-reported somatosensory responses along the neural hierarchy, with a special focus on the spinal cord and thus simultaneously recorded peripheral NAPs as well as SEPs from the spinal cord, brainstem and cortex to upper and lower limb stimulation. In the hand-mixed condition, we extracted the peripheral N6 (origin: median nerve), the peripheral N9 (origin: brachial plexus), the spinal N13 (origin: dorsal horn), the brainstem N14 (likely origin: cuneate nucleus) and the cortical N20 (origin: primary somatosensory cortex). In the foot-mixed condition, we extracted the peripheral N8 (origin: tibial nerve), the spinal

N22 (origin: dorsal horn), the brainstem N30 (likely origin: gracile nucleus) and the cortical P40 (origin: primary somatosensory cortex).

Replication was successful at all recording sites, where we observed response amplitudes that were highly significant at the group level (N = 36) and exhibited consistently large effect sizes (Table 1); to furthermore ensure the robustness of these results, we replicated them in Experiment 2 (Supplementary Table 1). Grand-average time-courses at the group-level are depicted in Figure 2 and delineate the temporal progression of the neurophysiological signal along the processing hierarchy, providing a robust and comprehensive view on somatosensory processing from periphery to cortex.

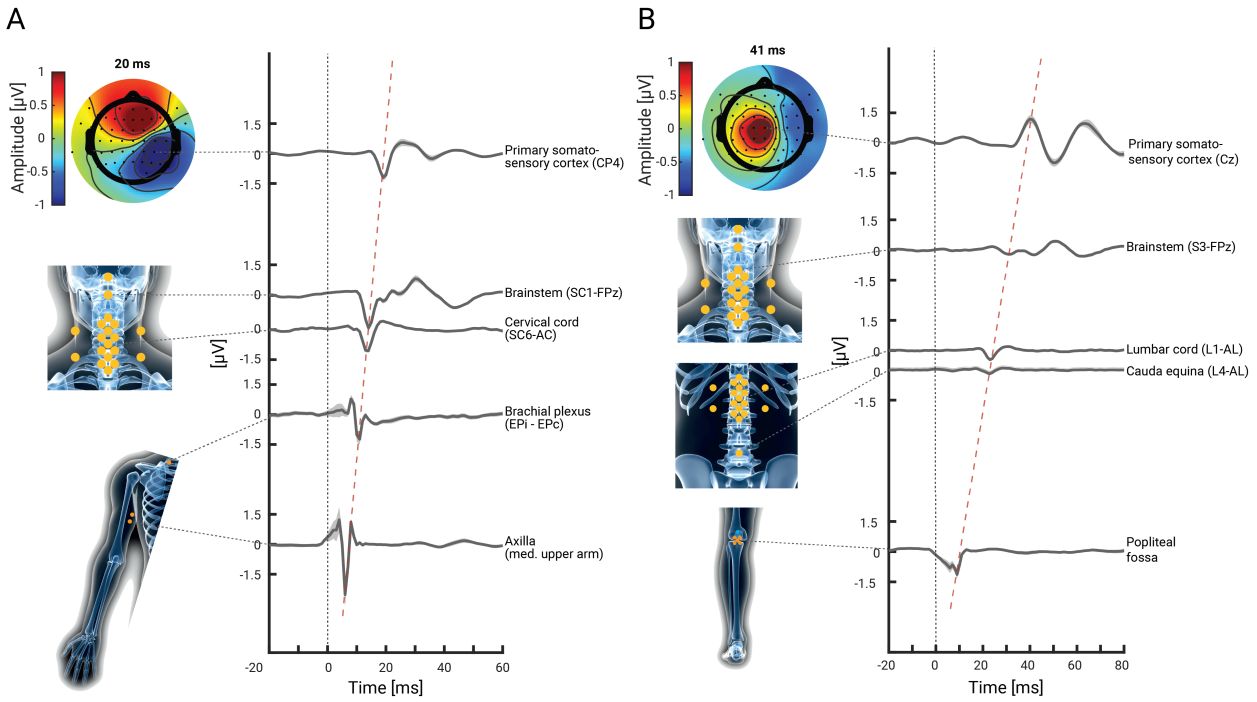

Figure 2. Grand-average NAPs and SEPs along the somatosensory processing hierarchy. *Group-level responses (N = 36) in the hand-mixed* ***(A)*** *and the foot-mixed* ***(B)*** *conditions of Experiment 1, with shaded error-bands depicting the standard error. The bottom two traces depict peripheral NAPs, the middle trace depicts spinal cord SEPs (referenced ventrally) and the top two traces depict brainstem and cortical SEPs. The grey dashed lines point to the electrode from which the data were obtained, the isopotential plots display the cortical topography and the red dashed line depicts the temporal progression of the signal along the neural hierarchy. The data underlying this figure can be found in the Supplementary Material (S1 Data).*

Table 1. Group-level statistics. *Descriptive statistics for SEP- and NAP-amplitudes, latencies and SNR (mean and standard error) and one-sample t-test of SEP- and NAP-amplitudes in the hand-mixed and foot-mixed conditions of Experiment 1. Note that the brainstem analysis (N14 / N30) is based on 30 participants only due to a technical problem (see Methods section; vr = ventral reference, tr = thoracic reference, CCA = canonical correlation analysis, # = number of participants with potentials visible at the individual level).*

SEP / NAP	#	Latency [ms]	Amplitude [µV / a.u.]	SNR	t	p	95%-CI	Cohen's d
Mixed median nerve stimulation (hand-mixed)								
N6	32	6.22 ± 0.09	-3.22 ± 0.55	14.09 ± 2.3	-5.89	<0.001	[-4.33; 2.11]	-0.98
N9	35	10.56 ± 0.15	-2.41 ± 0.21	8.8 ± 1.41	-11.55	<0.001	[-2.83; -1.99]	-1.92
N13 (tr)	36	13.25 ± 0.18	-0.85 ± 0.05	9.48 ± 1.16	-15.75	<0.001	[-0.96; -0.74]	-2.63
N13 (vr)	36	13.61 ± 0.17	-1.40 ± 0.08	17.38 ± 3.4	-17.01	<0.001	[-1.56; -1.23]	-2.84
N13 (CCA)	36	13.28 ± 0.17	-0.47 ± 0.03	21.58 ± 2.93	-16.93	<0.001	[-0.53; -0.42]	-2.82
N14	30	14.30 ± 0.19	-2.34 ± 0.14	24.19 ± 3.04	-16.95	<0.001	[-2.62; -2.06]	-3.09
N20 (CCA)	36	19.81 ± 0.20	-1.41 ± 0.06	23.66 ± 2.41	-21.85	<0.001	[-1.54; -1.28]	-3.64
Mixed tibial nerve stimulation (foot-mixed)								
N8	34	9.28 ± 0.16	-1.58 ± 0.18	10.23 ± 1.72	-8.64	<0.001	[-1.95; -1.21]	-1.44
N22 (tr)	36	23.83 ± 0.29	-0.80 ± 0.08	9.79 ± 1.72	-9.54	<0.001	[-0.97; -0.63]	-1.59

N22 (vr)	36	23.67 ± 0.35	-0.61 ± 0.06	14.14 ± 2.42	-10.42	<0.001	[-0.72; -0.49]	-1.74
N22 (CCA)	36	23.75 ± 0.29	-0.62 ± 0.06	31.28 ± 5.96	-10.74	<0.001	[-0.73; -0.50]	-1.79
N30	30	32.13 ± 0.43	-0.53 ± 0.04	6.57 ± 1.08	-13.29	<0.001	[-0.61; -0.45]	-2.43
P40 (CCA)	36	40.86 ± 0.38	1.42 ± 0.08	21.22 ± 2.07	18.17	<0.001	[1.26; 1.58]	3.03

Characterizing spinal SEPs in detail (Experiment 1)

Next, we aimed to provide a spatial, temporal and spectral characterization of spinal responses. First, the grand-average time-course of the potentials obtained from single, anatomically-defined target electrodes exhibited a tri-phasic shape with an initial positive deflection, a main negative deflection (at 13ms and 24ms, respectively) and a slowly decaying late positive deflection (red trace in Figure 3A and 3E). Second, our multi-channel set-up allowed for the first time to estimate the potentials' spatial topography (Figure 3B and 3F), which showed a radial dipole at peak latency, with a centre over the spinal cord, close to the spinal segments targeted by the electrical stimulation at wrist and ankle. Importantly, the topographies show that N13 and N22 responses are consistently limited to the relevant electrode-grid (cervical for upper-limb and lumbar for lower limb stimulation), with no evidence for responses in the irrelevant electrode grid, thus presenting a spatial double-dissociation. Third, grand-average time-frequency plots delineated responses with a frequency between ~50-320 Hz at the cervical and between ~50-250 Hz at the lumbar level (Figure 3C and 3G), demonstrating the fast nature of these potentials.

Considering recent findings on the complexity of somatosensory processing in the dorsal horn [2], we then went beyond the classical spinal SEPs and assessed whether we could detect responses that occur later than the early N13 or N22 components. Using a cluster-based permutation approach, we did indeed find statistical evidence for such late components: we identified a positive cervical cluster directly after the N13 component (17-35ms, p = 0.001; Figure 3D) and two lumbar clusters after the N22 (positive: 28-35ms, p = 0.002; negative: 126-132ms, p = 0.017; Figure 3H); two out of these three late potentials did also replicate in the independent sample from Experiment 2 (see Supplementary Material). Taken together, these results provide a comprehensive characterization of spinal SEPs, including responses that occur beyond the initial processing sweep in the spinal cord.

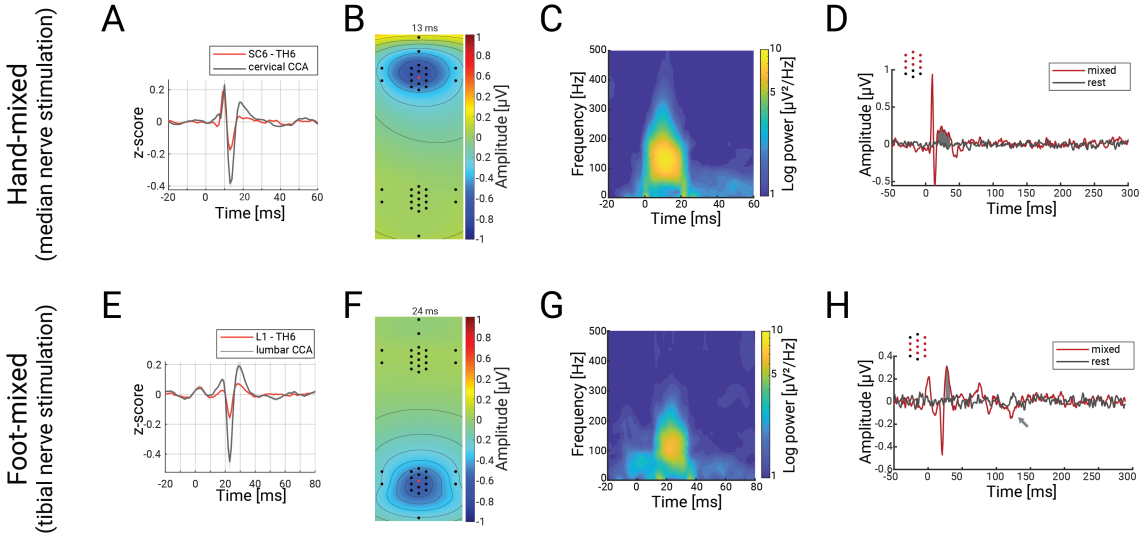

Figure 3. Spatiotemporal characterization of cervical and lumbar spinal cord potentials. *Panels **A-D** depict responses in the hand-mixed conditions and panels **E-H** depict responses in the foot-mixed condition. **(A)** and **(E)**: Grand-average SEPs across the group obtained from an anatomically-defined electrode (hand-mixed: 6th cervical vertebra; foot-mixed: 1st lumbar vertebra; red trace; both with thoracic reference over the spinous process of the 6th thoracic vertebra (TH6)) or after CCA (black trace), with both signals z-scored for comparison. Note the clear amplitude enhancement of the N13 and N22 after CCA. **(B)** and **(F)**: Grand-average isopotential plots (over all spinal channels) in the hand-mixed condition at the peak of the N13 **(B)**, and in the foot-mixed condition at the peak of the N22 **(F)**. **(C)** and **(G)**:*

Grand-average evoked time-frequency plots in the hand-mixed condition and the foot-mixed condition. ***(D)*** *and* ***(H)****: Results from cluster-based permutation testing for investigating late potentials. Depicted is the grand-average trace over all participants in the stimulation condition (hand-mixed / foot-mixed; red trace) and in simulated epochs from rest data (black trace), averaged over all channels that are part of the identified cluster (displayed as red dots on the top left). The gray areas depict the time-windows with significant differences and the gray arrow indicates an additional significant – but not replicable – potential (see also Supplementary Figure 1). The data underlying this figure can be found in the Supplementary Material (S2 Data).*

Enhancing sensitivity via multivariate spatial filtering (Experiment 1)

A main aim of our approach was to enhance the sensitivity for detecting spinal cord SEPs via a multi-channel setup and corresponding multivariate spatial filtering analyses, which provide two important benefits. First, multivariate spatial filtering approaches are able to enhance the SNR [41], which is critically important in scenarios such as the low SNR spinal recordings carried out here. Second, by reweighting the multi-channel signal on a participant-specific basis, they are able to account for between-participant differences of anatomy and physiology. This point is especially relevant in the spinal cord, where our results demonstrate that already at the group-level the anatomically-defined target channel (red dot in Figure 3B and F) does not necessarily capture the strongest deflection of the cervical N13 (slight rostral shift) or the lumbar N22 (slight caudal shift). With individual spatial shifts being even stronger, this indicates a necessity of having a grid of electrodes and correspondingly tailored analyses in order to be able to account for heterogeneity in source location and orientation.

We applied a variant of canonical correlation analysis (CCA) to the preprocessed data of the cervical or lumbar ESG grid, which is a multivariate method that takes information from all sensors of interest into account [40–42]. By finding participant-specific spatial filters that maximize the correlation between two multivariate datasets (here: single SEP trials and the trial-averaged SEP), it computes multiple orthogonal projections, of which we selected the strongest one with a temporal peak at the expected latency and a corresponding spatial pattern with the expected dipole orientation. The resulting group-level cervical N13 and lumbar N22 were similar in shape and latency but clearly exceeded the noise level compared to the single-electrode signal (black traces in Figure 3B and 3G), also resulting in a significantly higher SNR (more than two-fold increase in lumbar data; Table 1; Figure 4A and 4E), with a large majority of participants showing increased SNR after CCA. Most importantly, the CCA-induced SNR enhancement of the evoked responses allowed for the extraction of cervical and lumbar SEPs at the single-trial level in all participants: Figure 4B-D and 4F-H shows single-participant SEPs at the single-trial level, comparing the CCA projected data (right subpanels) with single-electrode data (left subpanels), clearly demonstrating the increase in signal-to-noise level in CCA-cleaned data. This indicates that taking the information from many channels into account provides a fundamental sensitivity increase for detecting even very weak – i.e. trial-wise – spinal responses.

Furthermore, in order to demonstrate that CCA is not creating artefactual signal due to overfitting, we carried out a control analysis. More specifically, in each participant we i) trained CCA on a random selection of 50% of the trials (underlying data: band-pass filtered, anterior-electrode re-referenced, epoched; time windows: 8-18ms for median and 14.5-29.5 for tibial nerve stimulation;), ii) saved the time-course of the first component, iii) repeated this procedure a thousand times and iv) then calculated all pair-wise absolute correlations between the obtained component time-courses (in the CCA training time-window). This procedure was also carried out on resting-state data, using identical trial timings. At the group level, we then compared the correlation strength between task-based data and resting-state data via a paired t-test. The main idea of this procedure was to demonstrate that correlations between subsampled CCA components would be substantially stronger in the presence of repeated evoked responses compared to CCA performed on the data from the resting-state data where we do not expect repeated evoked responses. For median nerve

stimulation, we obtained a group-average absolute correlation of 0.98 (range across participants: 0.76 – 1) in the task-based data and a group-average absolute correlation of 0.58 (range across participants: 0.46 – 0.73) in the resting-state data; for tibial nerve stimulation, the respective values were 0.96 (range: 0.61 – 1) for task and 0.50 (range: 0.37 – 0.68) for rest. Importantly, component correlations were significantly higher in task-based data than in resting-state data (median nerve stimulation: $t = 27.80$, $p < 9.5e\text{-}26$; tibial nerve stimulation: $t = 25.06$, $p < 3.1e\text{-}24$; one-tailed).

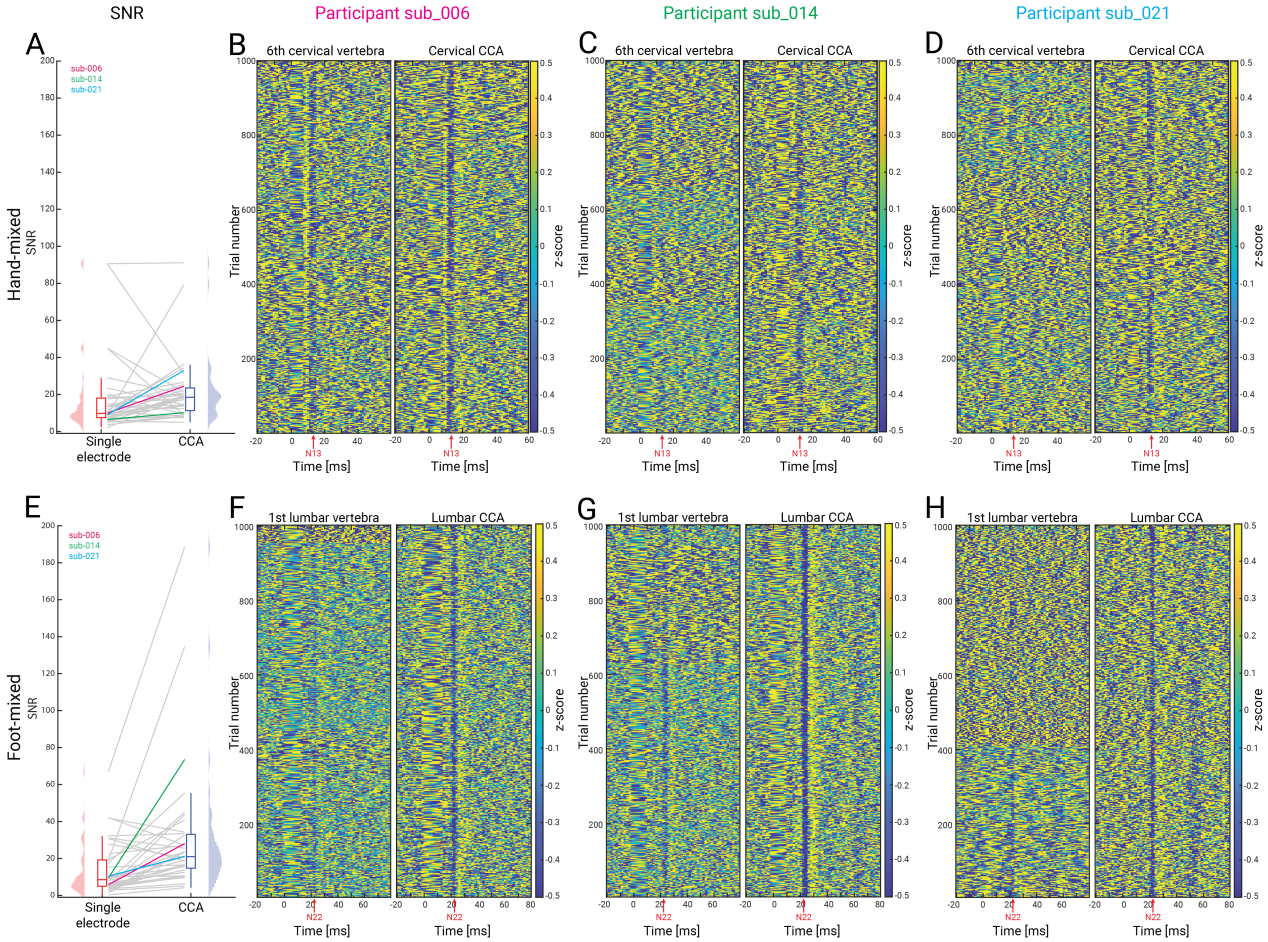

Figure 4. Comparing single-channel SEPs with canonical correlation analysis (CCA) SEPs. *Panels **A-D** depict responses in the hand-mixed conditions and panels **E-H** depict responses in the foot-mixed condition. **(A)** and **(E)**: signal to noise ratio (SNR) for responses obtained from single channels (6th cervical vertebra [upper] and 1st lumbar vertebra [lower]) and via CCA; note that the colored lines reflect the SNR of those participants that are displayed in the remaining panels. **(B-D)** and **(F-H)**: 1000 single trials of evoked responses (vertical axis) from three representative participants with responses obtained from an anatomically-defined electrode shown in the left subpanel and those from CCA shown in the right subpanel; the red arrow indicates the expected SEP latency (hand-mixed: N13; foot-mixed: N22). Note the clear increase in the potentials' single-trial visibility and consistency after CCA. The data underlying this figure can be found in the Supplementary Material (S3 Data).*

Detecting spinal SEPs to sensory nerve stimulation (Experiment 2)

Electrical mixed nerve stimulation at the wrist or ankle – as employed in Experiment 1 – produces the strongest SEPs in the somatosensory system, but is not an ecologically valid type of stimulation (e.g., due to antidromic conduction). To get one step closer towards natural stimulation, in Experiment 2 we additionally stimulated purely sensory nerve fibers of the fingers and toes (for details, see Figure 1). Using this more specific type of stimulation, we did indeed observe clear spinal SEPs, though now with an increased latency (4.3 and 7.6 ms delay for upper and lower limb stimulation, respectively) and reduced amplitude (approximately two-thirds for both upper and lower limb stimulation) compared to mixed nerve stimulation (Figure 5; Supplementary Table 2).

Such a pattern of results was similarly observed in peripheral NAPs and cortical SEPs for both finger and toe stimulation (Supplementary Table 2) and was also confirmed statistically (Supplementary Table 3). Similar to the above-reported mixed nerve results, applying CCA to spinal data resulted in an enhancement of sensory nerve SNR, allowing us to study characteristics of those responses as detailed in the following sections.

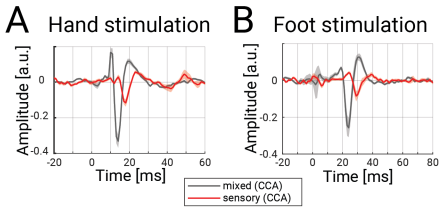

Figure 5. Spinal SEP to mixed and sensory nerve stimulation. *Depicted is the grand-average over all participants of Experiment 2 in* ***(A)*** *the cervical spinal cord to hand-mixed or fingers1&2 stimulation and* ***(B)*** *the lumbar spinal cord to foot-mixed or toes1&2 stimulation. All traces were obtained after CCA and the shaded error-bands reflect the standard error (the increased error-band around 0 ms in the lumbar data reflects remaining stimulus artifacts due to imperfect interpolation). The data underlying this figure can be found in the Supplementary Material (S4 Data).*

A first such example concerned a trial-by-trial investigation of our data (based on fitting linear-mixed-effects models), assessing whether changes in response amplitude across the processing hierarchy (from peripheral over spinal to cortical levels) would be fully explained by the stimulation condition or whether additional predictive links between the hierarchical levels would be detectable (Supplementary Material). In brief, we observed that the effects of different stimulation types propagated through the somatosensory processing hierarchy, jointly affecting the amplitudes of peripheral NAPs, spinal cord responses, and initial cortical potentials. Interestingly however, in the foot stimulation condition, additional condition-independent effects of spinal amplitudes on cortical amplitudes were observed, providing first evidence for a trial-by-trial spino-cortical link.

Probing integrative processing along the somatosensory hierarchy (Experiment 2)

Finally, we aimed to study a well-known phenomenon of integration in sensory processing, namely attenuation or gating effects, which are for example observed when stimulating two adjacent fingers: a neuronal response following simultaneous stimulation of both fingers is attenuated compared to the sum of neuronal responses to single finger stimulation. This effect of integrative processing is well studied at the cortical level and has been hypothesized to occur subcortically [43–45], yet unequivocal evidence for such integration occurring already at the spinal level is currently lacking. Therefore, we investigated attenuation effects along the processing hierarchy (i.e. at peripheral, spinal and cortical levels) and expected i) that peripheral NAPs would not show attenuation effects (considering that there are no synaptic relays yet), ii) that cortical SEPs would show such effects (replicating previous observations) and, most importantly, iii) that the enhanced sensitivity offered by our multi-channel spatial filtering approach would allow for uncovering such effects already at the spinal level.

We therefore obtained CCA-extracted amplitudes of cortical and spinal SEPs as well as peripheral NAPs to single-digit and simultaneous digit stimulation. CCA training and component selection was based on mixed nerve data (which have a higher SNR than sensory nerve data) and the chosen spatial filter was then applied to all sensory nerve conditions, ensuring independence of selection and testing. Using these unbiased amplitudes, we assessed the attenuation effect via interaction-ratios (IR): the IR is a measure that quantifies the amplitude reduction of the simultaneous digit stimulation compared to the arithmetic sum of the single-digit stimulations for each participant. Consistent across both upper and lower limb conditions, we obtained clear evidence for attenuation

effects not only at the cortical (N20 and P40), but also at the spinal level (N13 and N22); importantly, such effects were not evident at the peripheral level (N6 and N8; Table 2 and Figure 6). While cortical effect sizes of attenuation effects were strongest, spinal effect sizes were already substantial, i.e. in the medium to large range (Cohen's d of 0.5 for lower limb and 1.1 for upper limb). Taken together, our results indicate that robust attenuation effects in somatosensation are not an exclusively cortical phenomenon, but already occur at the level of the spinal cord, i.e. after the first synaptic relay.

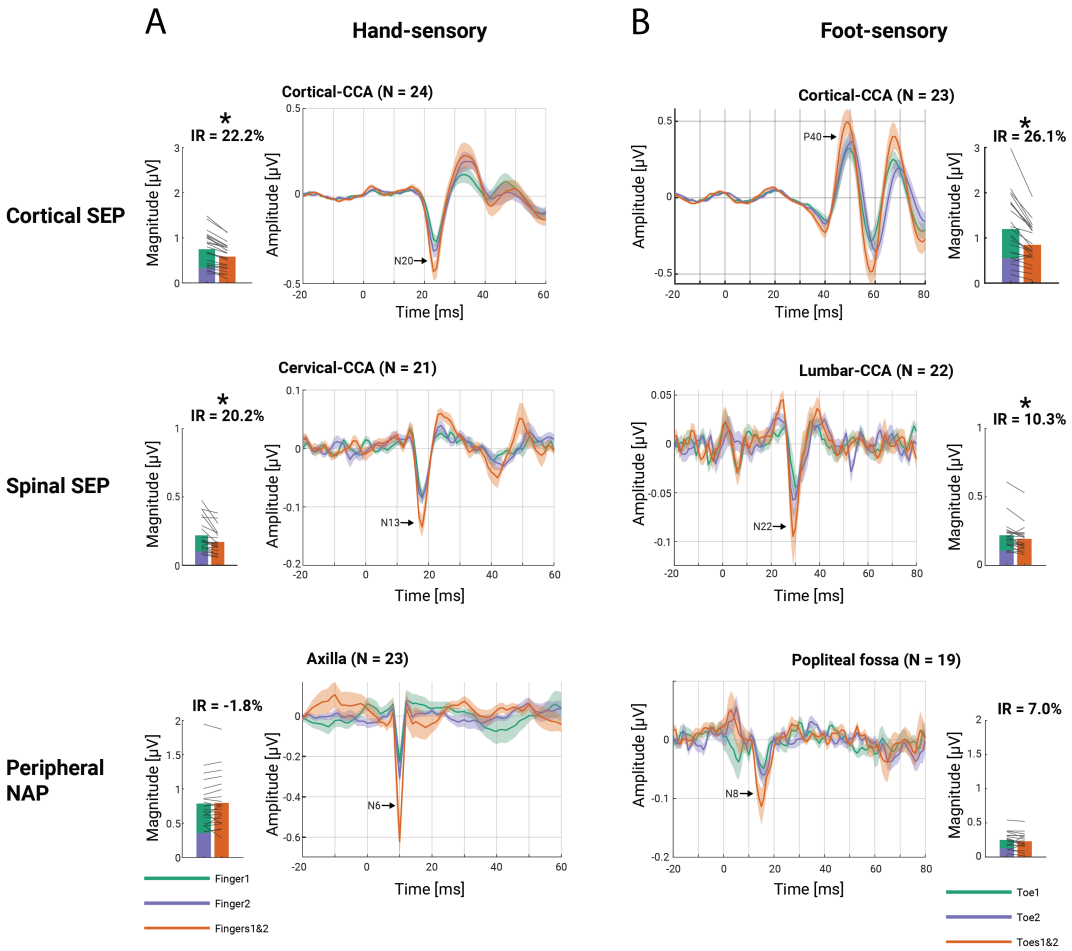

Figure 6. Attenuation effects along the processing hierarchy. *Potentials following finger stimulation* ***(A)*** *and toe stimulation* ***(B)*** *from top to bottom: cortical (N20/P40), spinal (N13/N22), and peripheral (N6/N8) responses. The traces in the middle columns display the grand-average response over participants to single-digit stimulation (green and blue traces) and double-digit stimulation (red trace), with the error-band displaying the standard error. The bar plots in the outer columns display the group-average of summed potential amplitudes to single-digit stimulation (green and blue bars) and double-digit stimulation (red bar), with grey lines depicting single-participant data. Note that i) slightly different numbers of participants entered analyses at the different levels (only those with identifiable and unbiased potentials), ii) the latency-terminology used here is based on mixed nerve latencies (sensory nerve potentials occur later), and iii) the scaling of the vertical axes is different between bar-plots and traces (as bar plots depict magnitude data and are based on extracted potential amplitudes at individually-optimized latencies). The data underlying this figure can be found in the Supplementary Material (S5 Data).*

Table 2. Group-level interaction-ratio results*. Tested were the interaction-ratios (IR) of SEPs and peripheral NAPs with a one-sample t-test.*

SEP / NAP	IR	tstat	p	95%-CI	Cohen's d
Hand sensory					
N6	-1.83%	-0.60	0.56	[-8.17%; 4.50%]	0.13
N13	20.25%	5.16	<0.001	[12.06%; 28.43%]	1.13
N20	22.21%	9.03	<0.001	[17.12%; 27.30%]	1.84
Foot sensory					
N8	6.99%	0.84	0.43	[-11.28%; 25.27%]	0.19
N22	10.25%	2.51	0.02	[1.76%; 18.75%]	0.54
P40	26.07%	6.56	<0.001	[17.83%; 34.32%]	1.37

Providing a resource for future experiments (Experiments 1 and 2)

Looking ahead, we also aimed to provide a resource for the planning of future experiments by establishing the robustness of the obtained spinal responses. Towards this end, we investigated how many trials are needed to obtain peak amplitudes significantly different from zero at the single-participant level (Figure 7A-H; left panels) and determined the joint minimal number of trials and participants needed for a significant effect at the group-level (Figure 7A-H; right panels) using resampling approaches.

The most immediately apparent effect is that no matter which outcome is considered, there is a clear order in the level of robustness across the different stimulation conditions, with mixed nerve stimulation giving more robust results than sensory nerve double-stimulation, which in turn leads to more robust potentials than sensory nerve single-stimulation. Thus, whereas in the mixed nerve condition with one target channel, one is almost guaranteed to obtain a significant group-level effect with e.g., ~10 participants and ~200 trials (Figure 7A-B), many more trials and / or participants would be required in the latter conditions to obtain a significant effect (Figure 7C-H). Despite this overarching trend, there is however also clear inter-individual variability in responses (cf. participant #1 and participant #13 in the hand-mixed condition, where approximately 100 vs 1000 trials were necessary to obtain a significant result in a majority of repetitions).

Another effect that is clearly visible is the beneficial effect of the CCA approach on the robustness of spinal SEPs: in contrast to employing an anatomically-defined target channel, employing CCA required smaller numbers of trials to obtain significant results for each participant in a consistent manner (but note that CCA was trained on the entire mixed-nerve data). While this is already visible at the individual-participant and group-level in the mixed nerve conditions (Figure 7A-B), it becomes even more apparent in the more SNR-limited sensory nerve conditions (Figure 7C-H). For instance, for single-digit stimulation of the index finger and an anatomically defined target channel (Figure 7E), the use of 24 participants and 1000 trials was necessary to obtain a significant group-averaged result with a probability of 0.8. In contrast, with the use of CCA (trained on 2000 trials of mixed-nerve data), either the same number of participants with only ~200 trials or 15 participants with ~500 trials were already enough to achieve similar results. These results thus allow researchers to make an informed decision on how to set up future experiments in terms of within- and across-participant factors.

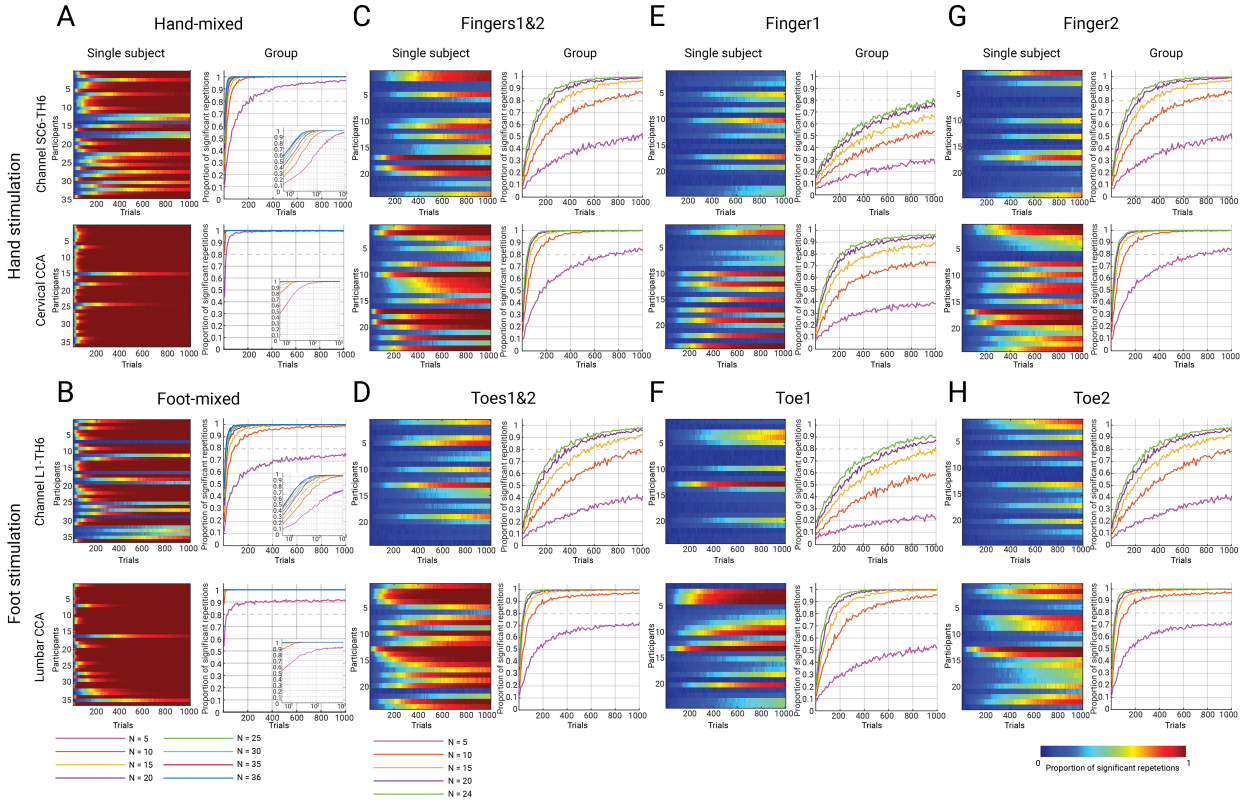

Figure 7. Robustness of spinal cord SEPs. *Heatmaps display the proportion of significant repetitions for each participant as a function of trial number and line plots display the proportion of significant repetitions as a joint function of trial number and sample size; data for the anatomically-defined target channel are in the top row and for CCA in the bottom row of each panel (insets for mixed nerve stimulation use a logarithmic scale to provide more details). The different conditions are displayed in the following panels: hand-mixed* ***(A)*** *and foot-mixed* ***(B)*** *(Experiment 1, N=36); hand-sensory (Experiment 2, N=24) with simultaneous finger stimulation* ***(C)****, and with single finger stimulations* ***(E and G)****; foot-sensory (Experiment 2, N=24) with simultaneous toe stimulation* ***(D)****, and with single toe stimulations* ***(F*** *and* ***H)****; for visual clarity, no more than 1000 trials are displayed.*

Recording of nociceptive spinal cord responses (Experiment 3)

In a final proof-of-principle experiment (N=7), we aimed to provide an example of the usability of this approach by recording spinal cord – and simultaneously also cortical – responses to nociceptive heat-pain stimulation (induced via a CO_2-laser). At the group level, we observed the canonical laser-evoked potentials (LEPs), i.e. the cortical N1 and N2P2 components, with the expected latency (Figure 8a). Most importantly, we also observed a distinct LEP at the spinal level, consisting of a negative deflection at 52ms (Figure 8b). This response could only be obtained by making use of our multi-channel set-up and spatial filtering approach, since it could not be detected in single electrode signals. Notably, this group-level response was consistent across data splits (four-fold split depicted in Figure 8c) and observed – with slight latency jitter – in every single participant (Figure 8d).

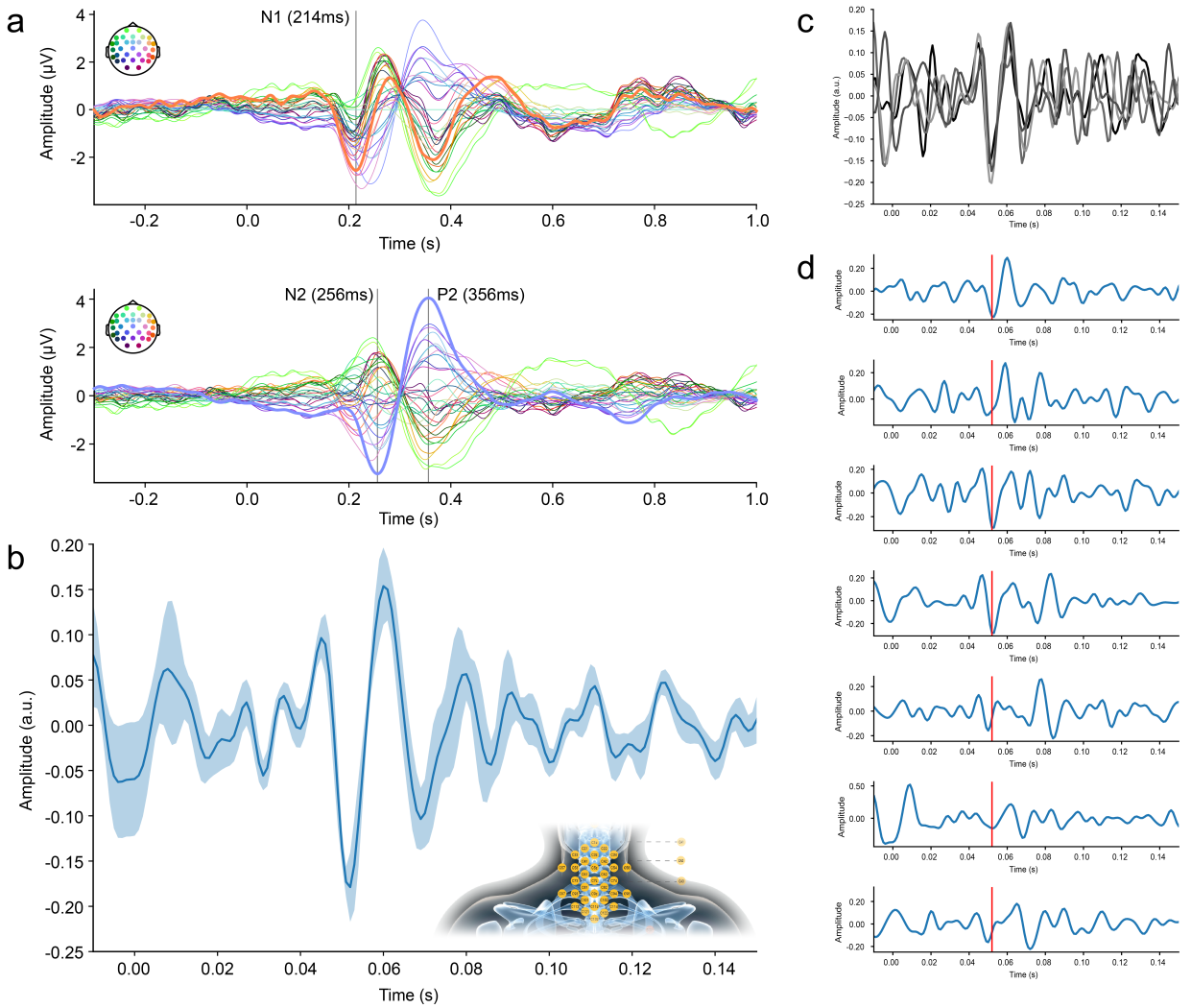

Figure 8. Cortical and spinal LEPs. *a) Grand-average (N = 7) cortical LEPs, obtained from single electrodes and consisting of N1 (latency: 214ms; data referenced to Cz) in the top row and N2P2 (latency: 256ms and 356ms; data referenced to average) in the bottom row; line colors correspond to the electrodes depicted schematically the top left of each panel, with thick lines corresponding to electrodes of interest (N1: T8, N2P2: Cz). b) Grand-average spinal LEPs, obtained from CCA and showing the most prominent deflection at 52ms. The thick line corresponds to the group-average of the first CCA component and the shaded band to the standard error of the mean across participants (amplitudes are in arbitrary units). The electrode patch of Experiment 3 is shown as an inset (anterior electrodes not shown). c) A four-fold split of trials (after having applied the spatial filter) shows a consistent response in each split at the previously shown latency (amplitudes are in arbitrary units and line colors reflect different splits). d) Single-participant (participants ordered from top (1) to bottom (7)) time-courses of the first CCA component, with the time-course of participant 2 having been multiplied by -1 (due to the polarity insensitivity of CCA); amplitudes are in arbitrary units. The red line indicates the time-point of maximal deflection observed in the group-level plot. The data underlying this figure can be found in the Supplementary Material (S6 Data).*

Discussion

Here, we report the development of a multi-channel electrophysiology approach to non-invasively record spinal cord responses with high precision and sensitivity, incorporating these responses within a comprehensive picture of processing along the somatosensory hierarchy (from peripheral nerves to somatosensory cortex). Across two separate experiments, we provide generalizable results by assessing spatiotemporal response properties in both the cervical and lumbar spinal cord, i.e. the targets of upper and lower limb projections. A central aspect of our approach concerns a reliable extraction and identification of spinal responses in a multivariate way, that is, reweighting the multi-

channel signal on a participant-by-participant basis using CCA, which enables single-trial estimation of spinal cord SEPs. In order to allow researchers from various fields to seamlessly build upon our results, we make all data as well as analysis code openly available and also carry out replication and robustness analyses, hoping to provide a status quo of what is currently feasible with multi-channel electrospinography.

Detailed characterization of spinal cord potentials

Spinal cord SEPs have been studied intensively in the last century, starting with their discovery in humans in an invasive study [46] and followed by non-invasive recordings [20–24]. Here, we employed a novel multi-channel approach (including specifically designed multichannel arrays) to expand upon findings from this large body of literature, which encompasses more than 150 publications in healthy humans, but where research had largely subsided.

First, we used a whole-body electrophysiology approach and simultaneously recorded peripheral, spinal, brainstem and cortical responses to electrical stimulation of a mixed nerve in the upper- and lower-limbs. This comprehensive recording set-up allowed us to embed spinal responses within the temporal progression of the neurophysiological signal along the entire somatosensory processing hierarchy. *Second*, we compared spinal SEPs following sensory nerve stimulation to those following mixed nerve stimulation and observed reduced peak amplitudes and increased latencies, likely due to the lower number of activated fibers and the additional travelling-distance of nerve impulses, respectively [47,48]. Reassuringly, even with single-digit stimulation (where only approximately 2000-5000 nerve fibres can be expected to be activated [49]), we observed mostly large effect sizes, hinting at the potential of our ESG approach to also record responses to ecologically more valid stimulation such as touch, which would be expected to have an even lower SNR. *Third*, we made use of our multi-channel setup to investigate the spatial distribution of cervical and lumbar SEPs: both presented as radial dipoles, slightly above the spinous process of vertebra C6 for the N13 and slightly below the spinous process of vertebra L1 for the N22 and with a sagittal center over the cord, speaking against a myogenic origin (which would be expected to result in a more lateralized distribution) [50]. Importantly, our results show a high degree of anatomical plausibility, not only by being centred close to the spinal segment of interest, but also by showing a spatial double-dissociation: the upper-limb N13 is clearly localized in cervical but not lumbar areas and the lower-limb N22 is clearly localized in lumbar but not cervical areas. To our knowledge, such a spatial characterization of spinal SEPs is unique, as even modern MSG-studies are limited to much smaller spatial windows [51,52] (for ESG, see[27]) and would thus not allow for such insights. Obviously, our data do not allow pinpointing the origin of these potentials within the spinal cord gray matter, but their post-synaptic nature has been established [32,53] and animal work suggests that they are generated by deep dorsal horn interneurons [54–56], likely as part of the post-synaptic dorsal-column (PSDC) pathway, which is a prominent source of input to the dorsal-column nuclei [57–59].

Finally, based on the recent evidence for extensive processing of afferent signals within the dorsal horn [2,3], we investigated the existence of late spinal potentials and indeed observed such SEP components following the cervical N13 (17-35ms) and the lumbar N22 (28-35ms). Similar late spinal potentials had been descriptively mentioned as part of a tri-phasic wave in some of the earliest invasive and non-invasive spinal recordings [20,21,60,61], but here we provide firm statistical evidence for their existence at the group-level for the first time. With respect to the origin of these late potentials, a myogenic source has been ruled out [61] and a contribution from late top-down brainstem potentials [44] is unlikely given their lumbar presence, rather pointing towards a local spinal origin, with a possible neurophysiological mechanism being primary afferent depolarization [56]. We further obtained tentative evidence for an ultra-late negative lumbar

potential following lower-limb stimulation after >100 ms. To our knowledge, no spinal SEPs have hitherto been reported at such latencies, although there are hints from early neuromagnetic neck recordings [62] and recent spinal recordings based on optically-pumped magnetometers [63] have also shown late spinal evoked fields. Taken together, the general possibility to detect late potentials opens the door for investigating local spinal processing going beyond a simple relay of information [2] as well as supra-spinal modulatory influences on processing in the dorsal horn [64] and here the millisecond resolution of our approach will be ideally suited to disentangle top-down from bottom-up effects.

Enhanced SNR and single-trial responses via multivariate spatial filtering

Traditionally, the analysis of SEPs from *ESG* data is based on acquiring a large number of trials, with most studies using single or very few spinal electrodes (though there are a few exceptions [21,28,65]) and then analysing *single-channel* data. Conversely, methodological advances in *EEG* data acquisition and analysis now allow for a better separation of signal from noise and use high-density *multi-channel* montages for construction of spatial maps, in which the data of the whole set of EEG electrodes is treated as a multivariate signal [66–69].

Our high-density ESG-montage thus enabled the application of methods that combine the information from many channels via spatial filters. Specifically, we used a CCA-based approach – that has previously been applied for extraction of early cortical SEPs [40–42,70,71] – and show that spinal SEP extraction is markedly improved with such a multi-channel spatial filtering approach. We believe this approach is especially beneficial for spinal data for two reasons. First, the ESG signal is particularly affected by physiological noise from cardiac and myogenic sources [21], leading to a low SNR with single-trial amplitudes usually hidden in background noise. Second, despite substantial inter-individual differences in the location of spinal segments relative to vertebrae [72,73], the latter are used as anatomical landmarks for electrode-placement. A spatial filter that compensates for such inter-individual differences will be beneficial for group-level analyses, but also for recovering signals in individual participants, where an electrode placed on a specific anatomical landmark might not capture the spatial peak of the response. Finally, because of volume conduction, potentials from the activation of spinal sources will be reflected in many electrodes and thus a simultaneous use of the signals from many electrodes may also potentially allow extraction of multiple sources when using multivariate methods.

By improving the SNR of ESG data, our spatial filtering approach allows not only for extracting more robust spinal SEPs, but also for studying the variability in spinal SEP amplitudes at single-trial level. While there are many benefits to this approach (see below), here we employed it to assess how trial-by-trial response amplitudes co-fluctuate across different processing levels. We observed that the effects of different stimulation conditions (i.e., single-digit, double-digit, and mixed nerve) corresponded to shared variance across the somatosensory processing hierarchy, encompassing peripheral NAPs, spinal SEPs, and early cortical SEPs. This covariance presumably reflected the number of stimulated nerve fibers (which varied between stimulation conditions) as well as the internal state of the activated neuronal populations. Yet additional condition-independent variations might be worth further investigation: during foot stimulation, spinal responses predicted cortical responses, providing a neurophysiological spino-cortical link on the single-trial level.

Integration effects are present already at the spinal level

Most importantly, we assessed a fundamental question of sensory processing, namely at which levels of the processing hierarchy information from the receptors is integrated, by testing for integrative processes at peripheral, spinal and cortical levels. In order to do so in a robust manner,

565 we used CCA to extract SEP amplitudes to single-digit and double-digit stimulation and quantified
566 the attenuation effect – a reduced response to double-digit stimulation compared to the summed-up
567 responses to single-digit stimulation – as a measure of integration. Integration effects were not
568 evident in the peripheral nervous system, where response amplitudes faithfully reflected the applied
569 stimulation. Conversely, significant integration effects with medium to large effect sizes were
570 evident consistently after the first synaptic relay, i.e. not only in cortex but already in the spinal
571 cord, the first processing station in the central nervous system. The cortical findings are in line with
572 several previous studies [43,45,74], but the robust spinal results – which were observed for both
573 upper and lower limb stimulation – go far beyond the previous literature, where only anecdotal
574 evidence of such effects existed at the cervical level [75,76]. While the simultaneous recording and
575 assessment of integration effects at peripheral, spinal and cortical levels is a first to our knowledge,
576 the observed progression of increasingly stronger integration effects along the neural hierarchy has
577 been suggested to be a consequence of increasing receptive field size [44].

578 Two mechanisms have been discussed to underlie integration effects: occlusion and lateral
579 inhibition [74,76,77]. Either mechanism could be at work in the spinal cord, considering the
580 integrative nature of many deep dorsal horn interneurons [2,3] as well as the receptive-field
581 organization of wide dynamic range neurons [78], both of which have been suggested to contribute
582 to the observed spinal SEPs [35,36,54,55]. Future work using experimental designs tailored to
583 dissociate these two mechanisms [74] might help to shed more light on the underlying processes at
584 the spinal level.

585

586 ***Assessment of nociceptive spinal cord responses***

587 In a final experiment, we demonstrated the versatility of our non-invasive approach by providing
588 corticospinal electrophysiological recordings of responses to nociceptive stimulation in a heat-pain
589 paradigm. While there is a multitude of EEG studies assessing cortical responses to various forms
590 of nociceptive stimuli (e.g. laser evoked potentials [LEPs; [79]], contact heat evoked potentials
591 [CHEPS; [80]], pinprick evoked potentials [PEPs; [81]]), a non-invasive assessment of spinal
592 responses to any type of nociceptive stimulation has hitherto not been reported to our knowledge.
593 In a first proof-of-principle experiment, we therefore leveraged the sensitivity increase afforded by
594 our multi-channel set-up to demonstrate concurrently recorded cortical and spinal LEPs. The spinal
595 response occurred at a time-point consistent with the activation of nociceptive A-delta fibres and
596 was observable to varying degrees in every single participant after spatial filtering.

597 While this first demonstration of non-invasively recorded spinal LEPs obviously awaits replication,
598 it is a promising step to investigate entire CNS mechanisms underlying the experience of pain in
599 health and disease. A non-invasive and direct window into spinal nociceptive processing is highly
600 relevant for pain research, considering that the spinal cord is not only the first CNS processing
601 station for nociceptive stimuli [82], but also a target of powerful descending control mechanisms
602 [83] and a structure often implicated in pain chronification [84].

603

604 ***Insights for future electrospinography experiments***

605 One outstanding question is how the advances introduced by our approach might benefit other fields
606 of human neuroscience, i.e. inspire new work on spinal cord function outside the domain of
607 somatosensation. An immediate experimental implication arises from the here-developed denoising
608 approach: while it was recognized early on that cardiac artifacts dominate the ESG signal [21] and
609 that massive trial-averaging or cardiac-gating was thus necessary, we instead achieved a direct
610 removal of the cardiac artefact via a denoising algorithm [85], eliminating these previous
611 limitations. This allows for example to deliver stimuli spaced across the cardiac cycle and we are

thus envisioning the use of our approach for investigating interoceptive processes, where spinal pathways are of importance for brain-body communication but not yet studied [86,87]. In addition, the sensitivity increase afforded by our multi-channel approach in combination with spatial filters is of benefit for domains where massive trial-averaging is impossible (e.g., in pain research due to ethical and safety reasons) or for experimental paradigms where only a few or even single trials are of interest (e.g., in deviance-detection designs).

Our approach could also provide clinical insights, considering that spinal pathologies are a core part of many neurological disorders, such as multiple sclerosis [6], spinal cord injury [5] or chronic neuropathic pain [7]. Relating to this, great strides have recently been made in the recovery of function after spinal cord injury and stroke via spinal neurostimulation [8,9,88,89]. Here, a non-invasive and temporally-resolved window on such processes – as provided by the CCA-enabled single-trial sensitivity – might offer mechanistic insights into processes underlying such recovery, especially considering the role of afferent input in the treatment of these maladies, as successfully characterized by our approach. Similarly, there are multiple initiatives aimed at developing biomarkers for analgesic drug development to target chronic pain [10,11,90,91] and considering that alterations in spinal processing are assumed to be a core feature of chronic pain development and maintenance [92–94], sensitive spinal recordings would be very helpful. In such endeavors, spinal SEPs could potentially serve as objective, non-invasive and innocuous biomarkers [35,36].

In any case, considering that underpowered studies are a troubling issue in neuroscience [95], both experimental and clinical studies that could arise from this work would need to be well-powered. In order to facilitate the planning of such studies, we provide group-level effect sizes, which – reassuringly – were similar across both experiments and mostly in the large range. In addition, we used resampling approaches on both data-sets to i) estimate the minimal number of stimuli to obtain a significant result at the participant-level and ii) jointly estimate the minimal number of stimuli and participants to obtain a significant result at the group-level. Simulating experiments this way allows for giving specific recommendations, such as that for mixed nerve stimulation acquiring ~200 trials in ~10 participants with single-channel recordings almost guarantees a significant group-level effect.

Finally, we hope that our non-invasive approach in humans will provide a macro-scale complement to research in animal models, where invasive recording techniques – such as multi-electrode recordings [96] or calcium imaging [97] – allow detailed and mechanistic insights into spinal processes occurring at the micro- and mesoscale. It is important to note that our approach of not only recording cervical, but also lumbar spinal cord responses could provide a unique across-species bridge, considering that the vast majority of spinal recordings in experimental animal models are carried out in the lumbar cord.

Limitations and comparison with other CNS-neuroimaging approaches

There are several limitations of our approach that are worth discussing. First, the supine positioning of participants might have led to a higher noise level in the ESG data due to electrode movements. While there are several alternative positions, we decided to record data in supine position based on extensive piloting, in which this position was reported to offer the most comfort over the course of the experiment without degrading data quality (e.g., due to tonic muscle activity). Second, we had hoped to reliably record brainstem SEPs arising from the cuneate nucleus (N14 [98]) and gracile nucleus (N30 [99]), as these are direct recipients of output from the spinal cord via the post-synaptic dorsal-column pathways [58]. Despite using optimal signal extraction leads, observing brainstem potentials was not possible in all conditions, mainly due to the limited SNR to digit stimulation. Third, it is important to point out that this study introduced a novel methodological approach and was thus focused on the detection of spinal responses to carefully-controlled stimulation that gives

rise to a strongly-synchronized high-amplitude signal. One might therefore ask whether this method will perform well under more naturalistic conditions, such as mechanical or thermal stimulation. We believe that the combination of methodological improvements introduced here should also be helpful in such low-SNR scenarios, as already demonstrated exemplarily for single-digit stimulation. Finally, it should also be noted that there is some loss of objectivity when using CCA, considering that a-priori knowledge informed the time-period for training CCA and the choice of component – this might be alleviated in the future by developing automated procedures based on pre-defined criteria.

In terms of comparison with other neuroimaging methods for assessing the entire CNS, we note that only fMRI and MEG (based on optically pumped magnetometers [OPMs]; [100,101]) have so far been used for simultaneous assessment of cortico-spinal processes. While corticospinal fMRI – as employed for studying the interactions between supraspinal and spinal structures that underlie resting-state connectivity [102,103], motor control [104,105] or top-down modulation of nociceptive processing [106,107] – offers unparalleled spatial resolution, it is an indirect measure of neuronal processes with ensuing low temporal resolution. Here, our approach would provide an important complementary assessment, as it would for example allow for a temporally precise delineation of possible interactions between top-down and bottom-up responses at the spinal level due to its millisecond resolution. OPM-MEG has recently been employed in a proof-of-principle study to simultaneously record spinal and cortical somatosensory-evoked responses similar to those investigated here in Experiment 1 [63] (see [108] for corticospinal recordings during a motor task). While the high costs and limited bandwidth of many OPM sensor types currently limit widespread adoption (especially when interested in very fast spinal responses as investigated here), the wearable nature and flexible arrangement possibilities of OPM-MEG make this a very promising methodological approach for entire CNS assessments with high temporal precision.

Outlook

In conclusion, we established an approach for the non-invasive recording of spinal cord responses that should be readily-accessible and widely-available, addressing a previously missing link in the study of reciprocal brain-body communication. Our method provides direct recordings of electrophysiological responses with high temporal precision (allowing to investigate different response components, i.e., early and late potentials), has a high sensitivity due to the multivariate combination of spinal multi-channel data (enabling single-trial estimates), and is integrated with the recording of afferent and efferent signals (peripheral and supra-spinal responses). We believe that this approach could be extended to other settings of natural stimulation – such as social touch or pain (for which we provide initial evidence) – and is not only suitable for investigating hard-wired bottom-up processing, but also its modulation by various factors, such as signal integration as demonstrated here to already take place in the human spinal cord. We thus hope to have provided a comprehensive approach that allows for a sensitive and direct assessment of spinal cord responses at millisecond timescale in various fields beyond somatosensation and anticipate its use in the context of interrogating the spinal cord's role in the interplay of bottom-up and top-down processes that together give rise to our sensations in health and disease.

Materials and Methods

Participants

Experiment 1. 42 healthy right-handed volunteers participated in this experiment. Two participants were not able to successfully complete the experiment (cigarette craving in one case, bathroom use

in another case) and their data were thus discarded. Four participants were excluded due to absent peripheral potentials, leading to a final sample size of 36 participants (18 female; age: 25.5 ± 3.5 years (mean ± SD)). All participants provided written informed consent and the study was approved by the Ethics Committee at the Medical Faculty of the University of Leipzig. Please note that the final sample-size of 36 participants was specified in a pre-registration prior to the start of the study and was chosen in order to detect a medium-sized effect (Cohen's d = 0.5) with a power of 90% (at an alpha-level of 0.05 with one-tailed testing).

Experiment 2. 26 healthy right-handed volunteers participated in this experiment. Two participants were excluded due to absent peripheral potentials in the mixed nerve stimulation condition, leading to a final sample size of 24 participants (12 female; age: 24 ± 4.5 years (mean ± SD)). All participants provided written informed consent and the study was approved by the Ethics Committee at the Medical Faculty of the University of Leipzig. Please note that the final sample size of 24 participants was specified in a pre-registration prior to the start of the study. This was based on a power calculation of data from of the 36 participants in Experiment 1, where we observed an effect size of d = -0.85 for median mixed nerve stimulation and of d = -0.62 for tibial mixed nerve stimulation (in 30 Hz high-pass-filtered, but otherwise uncleaned, data). Taking the smaller of these two effect sizes, and aiming for a power of 90% (at an alpha-level of 0.05 with one-tailed testing) resulted in a necessary sample size of 24 participants. Although we were using results obtained from mixed nerve stimulation as the basis for our power calculation (which is known to result in stronger responses than those from stimulation of a purely sensory nerve), we employed a conservative way to estimate our effect size: i) we used raw data that was only preprocessed by a high-pass-filter, ii) we based our power calculation on the lumbar potential that is possibly more difficult to detect, and iii) we selected the same electrode in each participant (cervical: SC6, lumbar: L1) to calculate the group statistics, which is rather conservative especially for the lumbar channels, because the location of the lumbar segments of the spinal cord differs extensively between participants [73].

Experimental Design

We conducted two experiments in which human participants received electrical stimuli to mixed or sensory parts of an arm and of a leg nerve. In Experiment 1, only mixed fibers were stimulated, specifically of the median nerve at left wrist and of the tibial nerve at the left ankle. In Experiment 2, the same mixed nerve stimulation was applied, and additionally sensory parts of the nerves were stimulated (two fingers or two toes). In both experiments electrophysiological signals were recorded at different levels of the processing hierarchy – at the peripheral nerve, the lumbar and cervical spinal cord, the brainstem and the cortex.

Experiment 1. The experiment had a repeated-measures design, meaning that each participant underwent all experimental conditions. The experiment consisted of two conditions, named hand-mixed and foot-mixed in the following. In the hand-mixed condition, the left hand of the participant was stimulated with electrical pulses to the median nerve at the wrist. In the foot-mixed condition, the left foot of the participant was stimulated with electrical pulses to the posterior tibial nerve at the ankle. We refer to these conditions as 'mixed', because at the wrist and the ankle, the median and tibial nerve, respectively, are mixed nerves, i.e., contain both sensory and motor nerve fibers. Figure 1A displays the experimental timeline of Experiment 1.

Experiment 2. Similar to Experiment 1, this experiment also had a repeated-measures design, though now consisting of eight conditions, named hand-mixed, finger1, finger2, fingers1&2, foot-mixed, toe1, toe2, and toes1&2. The hand-mixed and foot-mixed conditions were the same as in Experiment 1 (except for differences in the inter-stimulus-interval and being presented completely in one block each). In the finger stimulation conditions, the index and middle finger of the

participant's left hand were stimulated with electrical pulses. These pulses could occur in three different ways: to the index finger only (finger1), to the middle finger only (finger2), or to both fingers simultaneously (fingers1&2). In the toe stimulation conditions, the first and second toe of the participant's left foot were stimulated with electrical pulses either to the first toe only (toe1), to the second toe only (toe2), or to both toes simultaneously (toes1&2). We refer to all finger and all toe stimulation conditions also as 'hand-sensory' and 'foot-sensory' conditions, because at the fingers and the toes, the median and the stimulated branches of the posterior tibial nerve contain only sensory nerve fibers. Figure 1B displays the experimental timeline of Experiment 2.

Electrical stimulation

Experiment 1. The electrical stimulus was a 0.2 ms square-wave pulse delivered by two constant-current stimulators ("DS7A", Digitimer Ltd, Hertfordshire, UK; one stimulator for each nerve) via a bipolar stimulation electrode with 25 mm electrode distance ("reusable bipolar stimulating surface electrode", Spes Medica, Genova, Italy) to the left median or the left posterior tibial nerve, respectively. The stimulation electrodes were placed (with the cathode being proximal) at the palmar side of the wrist (median nerve stimulation) and at the median side of the ankle (posterior tibial nerve stimulation). The stimulation intensity was set to just above the individual motor threshold, which was defined as the intensity at which a participant's thumb or first toe started to twitch (visually determined). All participants perceived the stimulation intensity as a distinct, but not painful, sensation.

Experiment 2. Equipment and electrode placement for mixed nerve stimulation was identical to what is described above for Experiment 1. For finger or toe stimulation, ring electrodes ("digital electrode for recording and stimulation", Spes Medica, Genova, Italy) were attached with the cathode being proximal to participants' left index finger and left middle finger as well as left first toe and left second toe. While we intended to stimulate mixed and sensory parts of the same nerve, when stimulating the fingers or toes, it is not possible to clearly differentiate which nerve is stimulated, since there is an individual variability in the spatial distribution of the dermatomes [109,110]. Therefore, it is important to keep in mind when interpreting our results that during stimulation of the index and middle finger, sensory fibers of the median as well as the ulnar and radial nerve might be stimulated (lower limb: sensory fibers of the superficial and deep peroneal nerves). Each of the fingers or toes were stimulated by a different stimulator. The stimulation intensity was set to three times the detection threshold, which was determined via the method of limits. If necessary, i.e., if participants reported to experience the stimulus as less intense over time, the stimulation intensity was slightly increased in-between stimulation blocks based on experience from pilot experiments as well as suggestions by earlier work [111]. The applied intensity was never perceived as being painful.

Electrographic recordings

Experiment 1. All electrographic signals were recorded with TMS-suitable Ag/AgCl electrodes ("TMS-compatible multitrodes", Easycap GmbH, Herrsching, Germany). For electroencephalography (EEG), 64 electrodes were arranged on an EEG cap (Easycap GmbH) with standard positions according to the 10-10 system and referenced to the right mastoid (RM). Recorded EEG- channels were: Fp1, Fp2, F3, F4, C3, C4, P3, P4, O1, O2, F7, F8, T7, T8, P7, P8, AFz, FCz, Cz, Pz, FC1, FC2, CP1, CP2, FC5, FC6, CP5, CP6, FT9, FT10, LM (left mastoid), Fz, F1, F2, C1, C2, AF3, AF4, FC3, FC4, CP3, CP4, PO3, PO4, F5, F6, C5, C6, P5, P6, AF7, AF8, FT7, FT8, TP7, TP8, PO7, PO8, FPz, CPz, F9, and F10. An active ground electrode was placed at POz.

For electrospinography (ESG), 39 electrodes were placed on the upper body, with the largest part of the electrodes placed into one cervical and one lumbar electrode patch. These patches were custom-made and consisted of the same fabric used for the EEG cap (kindly provided by Easycap GmbH). ESG data was referenced to an electrode positioned over the spinous process of the 6th thoracic vertebra (TH6) and the following electrodes were located at anatomical positions: electrode SC1 at the 1st cervical vertebra, electrode SC6 at the spinous process of the 6th cervical vertebra, electrode L1 at the spinous process of the 1st lumbar vertebra, and electrode L4 at the spinous process of the 4th lumbar vertebra. An additional 16 electrodes were organized in a grid around each one of the two spinal target electrodes SC6 and L1 (Figure 1). The grid organization, which was developed in pilot experiments, aimed at capturing the spatial distribution of the spinal signal. The midline of this grid was positioned vertically on the spine and consisted of 5 electrodes (the 3rd one being the spinal target electrode) with a vertical inter-electrode distance of 2 cm. Two further vertical lines of 4 electrodes each were placed 1 cm to the right and left of the midline electrodes and another two vertical lines of two electrodes each were placed 5 cm to the right and left of the midline. In addition to these dorsally placed electrodes, there were two ventrally placed electrodes – one supra-glottic (AC) and one supra-umbilical electrode (AL). Such ventral electrodes have been described to be beneficial for SEP extraction in the literature [26,27,112,113]. Because the EEG and ESG montage used different references, we added Fz to both montages with channel name "Fz" in the EEG montage and "Fz-TH6" in the ESG montage, as this allows to combine the two montages into one by re-referencing at a later point. In 6 out of the 36 participants (sub-001 to sub-006) Fz-TH6 was missing in the ESG setup due to a technical error. The active ground electrode stabilized the signal via the "driven right leg" principle. It was placed at POz in the EEG montage and in the middle between TH6 and S20 in the ESG montage. Please see also our reasoning regarding the placement of the spinal reference in the Supplementary Material.

In addition to EEG and ESG, we also recorded several other types of data. First, electroneurographic (ENG) data – i.e., peripheral nerve action potentials (NAPs) – of the median nerve were recorded at the level of the left axilla (over the biceps, reference electrode proximal, distance 3 cm between electrodes) and the left Erb's point (referenced to right Erb's point). Peripheral NAPs of the posterior tibial nerve were recorded from the popliteal fossa (with 5 electrodes: one electrode was placed in the center of the fossa and 4 electrodes around it at a distance of 1 cm; all knee channels were referenced to a 3 cm proximal electrode). Second, electrocardiographic (ECG) data were recorded from an electrode placed at the left lower costal arch and referenced to a right sub-clavicular electrode. Third, electromyographic (EMG) data were recorded at the hand from the abductor pollicis brevis muscle and at the foot from the flexor hallucis brevis muscle, with the EMG electrode being placed over the muscle belly and the reference electrode being proximal (please note that EMG data are not reported in this manuscript). Fourth, we recorded the participants' respiratory activity (with a respiration belt: "reusable respiratory effort sensor", Spes Medica S.r.l., Genova, Italy; data also not reported here).

We aimed at keeping impedances at all electrodes below 10 kOhm. All electrographic signals were recorded with NeurOne Tesla amplifiers and software (Bittum Corporation, Oulu, Finnland), applying an anti-aliasing filter at 2500 Hz with a lower cutoff at 0.16 Hz and sampled at a rate of 10000 Hz.

Experiment 2. The employed recording equipment as well as the ESG, ECG and ENG electrode placement was identical to what is described above for Experiment 1. EEG was recorded using 39 electrodes arranged on an EEG cap with standard positions according to the 10-10 system and referenced to the right mastoid (RM). Recorded EEG-channels were: Fp1, Fp2, F3, F4, C3, C4, P3, P4, O1, O2, F7, F8, T7, T8, P7, P8, AFz, Fz, Cz, Pz, FC1, FC2, CP1, CP2, FC5, FC6, CP5, CP6, LM (left mastoid), FCz, C1, C2, FC3, FC4, CP3, CP4, C5, C6, and CPz. The electrooculogram was placed lateral to the outer canthi (EOGH) and in the center below (EOGV) the right eye and used

the same reference as EEG. An active ground electrode was placed at POz. EMG was not recorded in this experiment.

Experimental procedure

Experiment 1. First, the EEG, ESG, ENG, EMG, and ECG electrodes were attached to the participant's skin. Next, the respiration belt was attached at the level of the $9^{th}/10^{th}$ rib. Then participants were asked to lay down on a cushioned bench on their back in a semi-darkened and acoustically shielded EEG-cabin. For participant comfort, the head support of the bench was slightly raised and a cushion roll was placed under their knees. Next, electrical stimulation location and intensity were determined and participants were instructed to look at a fixation cross during the stimulation blocks, which was attached to the ceiling. The experiment started with 5 minutes of resting-state recording (eyes open) followed by eight stimulation blocks, each consisting of 500 stimuli. During one block, stimuli were delivered to one nerve only, i.e., either the median or the posterior tibial nerve (thus, there were four median and four posterior tibial nerve stimulation blocks in total). The stimulation blocks were presented in alternating order and the order was counterbalanced across participants. Another two blocks of similar length followed at the end of the experiment – these are not discussed here as they were part of another project and are thus explained in further detail elsewhere [71]. We used an inter-stimulus-interval of 763 ms with a uniformly distributed jitter of +/– 50 ms in steps of 1 ms. Taken together, each nerve received 2000 stimuli overall. The experiment took approximately 5.5 - 6 hours, with the presentation of the experimental stimulation blocks (including breaks) taking approximately 90 minutes.

Experiment 2. Since the attachment of the recording equipment to the participants and the instruction of the participants were identical to Experiment 1, in the following we only list details specific to Experiment 2. Before each experimental block started, the individual stimulation intensity was adjusted if necessary. The experiment started with 5 minutes of resting-state recording followed by 10 stimulation blocks (with short breaks between blocks). There were four different types of stimulation: i) mixed nerve stimulation of the median nerve (1 block), ii) mixed nerve stimulation of the tibial nerve (1 block), iii) sensory nerve stimulation at the fingers (4 blocks), and iv) sensory nerve stimulation at the toes (4 blocks). All blocks of one stimulation type were presented in a row (with pauses between blocks) but the order in which the four stimulation types were presented was balanced across subjects. There was one block for hand-mixed and one block for foot-mixed stimulation and each of these blocks contained 2000 stimuli. Sensory nerve stimulation was separated into four blocks (1500 stimuli each) of finger and four blocks (1500 stimuli each) of toe stimulation. During each finger stimulation block, finger1, finger2, and fingers1&2 were stimulated in a pseudo-random order, such that each of the three stimulation conditions occurred 500 times. The same procedure was employed for the toe stimulation blocks, with the only difference that toe1, toe2, and toe12 were stimulated in pseudorandom order. Each type of digit stimulation (finger1/toe1, finger2/toe2, fingers1&2/ toes12) thus consisted of 2000 stimuli. All stimuli were delivered with an inter-stimulus-interval of 257 ms with a uniformly distributed jitter of +/- 20 ms in steps of 1 ms. The experiment took approximately 6-6.5 hours, with the presentation of the experimental blocks (including breaks) taking approximately 90 minutes.

Data processing and statistical analysis (Experiment 1)

Unless noted otherwise, all data were analyzed using MATLAB R2019b (The MathWorks Inc., Natick, Massachusetts, USA) and the EEGlab toolbox [114].

Stimulation artifact removal. Electrical stimulation of peripheral nerves as employed here induces an artifact in all channels at the time point of stimulation and was removed by interpolation (using

a piecewise cubic hermite interpolating polynomial). Since the temporal spread of this artifact differed among participants, as well as in cervical and lumbar channels, we defined individual artifact windows for cervical and lumbar levels by finding the beginning and the end of the artifact in the average over all trials and all cervical or lumbar ESG channels. At the cervical level, average artifact windows ranged from -1.8 ms (SD = 0.8 ms) to 4.4 ms (SD = 1.4 ms) and at the lumbar level from -2.9 ms (SD = 1.4 ms) to 7.1 ms (SD = 2.8 ms).

EEG data preprocessing. First, the stimulation artifact was interpolated using the previously identified cervical artifact windows and the continuous EEG signal was down-sampled to 1000 Hz (anti-aliasing filter with cutoff at 0.9 and transition bandwidth at 0.2). *Second*, artifact sources were identified in the signals using ICA. For this, overly noisy channels were removed from the signal – based on visual inspection of the power spectral density and the trial-based root mean square activity in each channel – and interpolated (this was the case for one channel in five participants). Zero-phase IIR filtering was then applied to the continuous concatenated signal from all stimulation blocks (i.e., median and tibial nerve stimulation), consisting of a high-pass filter at 0.5 Hz and a low-pass filtered at 45 Hz (Butterworth, 4th order). On the filtered signal, independent component analysis (ICA, Infomax [115]) was performed and ICs reflecting eye blink, heart and muscle artifacts were identified. *Third*, ICs identified as representing artifactual sources were removed from the EEG signal preprocessed in the same ways as for ICA, with the difference that it i) consisted of concatenated blocks of each stimulation condition only (i.e., hand-mixed or foot-mixed) and ii) was zero-phase IIR filtered with a notch (48-53 Hz) and a band-pass (30-400 Hz) Butterworth filter of 4th order. *Fourth*, the ICA-cleaned signal was re-referenced to average reference and remaining noisy time points were identified in lower frequencies (1 - 15 Hz) using a threshold of 5 standard deviations and in higher frequencies (15 - 45 Hz) using a threshold of 60 µV. If more than 50% time points were identified in one channel, this channel was removed from the data and interpolated. In one participant 7 channels were removed from the hand-mixed condition and in another participant 18 channels were removed from the foot-mixed condition. *Fifth*, the cleaned signal was cut into epochs from 200 ms before to 700 ms after stimulus onset and baseline-corrected (with a reference interval from -110 ms to -10 ms before stimulus onset). In the hand-mixed condition, this procedure led to an average of 97.9% remaining trials (range across participants: 886 trials to 2000 trials) and in the foot-mixed condition to an average of 97.5% remaining trials (range across participants: 992 trials to 2000 trials).

ESG data preprocessing. After the stimulation artifact was interpolated in the individually defined cervical and lumbar artifact windows, the ESG data were down-sampled to 1000 Hz.

Since ESG data are known to present with severe cardiac artifacts [21], we aimed to correct for these. In each participant, we therefore first identified R-peaks in the ECG channel using an automatic procedure provided by the FMRIB plugin for EEGlab (https://fsl.fmrib.ox.ac.uk/eeglab/fmribplugin/), which was followed by visual inspection and manual correction if necessary. Next, the heart artifact was removed from each ESG channel separately, using an approach that is a modification of a method previously developed for removing ballistocardiographic artifacts in simultaneous EEG-fMRI recordings [85]. First, a principal component analysis (PCA) was applied to a matrix of all heart artifacts (artifact x time) in one channel, with the time window of each heart artifact ranging from –0.5 * median(RR) to +0.5 * median(RR) around each R-peak (with RR referring to the interval between R-peaks, i.e., the heart-period). Then, an optimal basis set (OBS) was created based on the mean heart artifact and the first 4 components obtained from the PCA. Finally, this OBS was fitted to each heart artifact and then removed from it.

After correction for cardiac artifacts, noisy channels were identified via visual inspection of the power spectral density and one channel in five participants was removed (no interpolation of missing channels was performed at the spinal level).

The analysis steps described below were performed in the concatenated blocks of one condition (rest, hand-mixed or foot-mixed) and, because we wanted to investigate SEPs with different references, were carried out separately for differently referenced datasets. In addition to the recording reference located over the spinous process of the 6th thoracic vertebra (TH6), we also made use of a ventrally located reference, because it has been reported that this can be beneficial for SEP extraction [26,112] – the ventral reference was channel AC in the hand-mixed and channel AL in the foot-mixed condition. *First*, a zero-phase IIR filtering was applied to the data with a notch (48-53 Hz) and a band-pass (30-400 Hz) Butterworth filter (4th order). *Second*, time points with absolute ESG activity above 100 µV were removed from the continuous data. If in one channel more than 50% of time points were identified, the whole channel was excluded instead. No further channels were removed and together with the channel exclusion based on the spectrum in the whole sample an average of 0.1 channels were removed (SD = 0.4). *Third*, the signal was cut into epochs with the same time range as reported for the EEG signal (from -200 ms to 700 ms around stimulus) and epochs were baseline-corrected (reference window -110 ms to -10 ms before stimulus onset). In the hand-mixed condition, 93.7% of trials remained in the data set on average (range across participants: 1210 trials to 2000 trials) and in the foot-mixed condition, 93.6% trials remained (range: 1193 trials to 1997 trials).

For the investigation of late potentials, the signals were pre-processed in the same way as described above, except that the reference was kept at the recording reference (at TH6) and the band-pass filter was set to 5-400 Hz.

ENG data preprocessing. The peripheral NAPs of interest have very short latencies (i.e., occur almost immediately after the electrical stimulation), meaning that in some participants the interpolation windows defined at the cervical or lumbar level might be too wide and thus contain the NAPs of interest. Therefore, in order to remove the stimulation artifact, but retain the NAPs, the ENG data were interpolated in a time window from 1.5 ms before to 4 ms after stimulus onset. Data were then down-sampled to 1000 Hz, band-pass and notch filtered in the same range as ESG data and cut into epochs and baseline-corrected (with the same epoch and baseline windows used for ESG data).

CCA. In order to enhance the signal-to-noise ratio and also allow for single-trial analysis, we made use of our multi-channel setup and applied canonical correlation analysis (CCA) to EEG and to the ventral referenced ESG data, separately for the mixed median and tibial nerve stimulation conditions. In the context of EEG, CCA has for example been used as blind source separation approach to remove noise such as muscle activity [116] and as a technique to improve single-trial classification of evoked potentials [117]. In both cases, the goal is to obtain a spatial filter and consequently a projected component with the largest similarity between two data matrices. Inverting a spatial filter creates corresponding topographies which can then be interpreted in a neurophysiologically meaningful manner [118]. We employed a variant of CCA as used previously for single-trial extraction in EEG data[40–42], also known as canonical correlation average regression [41]. For two multi-channel signals X and Y, CCA finds the spatial filters w_x and w_y that maximize the correlation

$$\max_{w_x, w_y} corr\left(w_x^T X, w_y^T Y\right).$$

While both multi-channel matrices X and Y have the same size with the structure channel × time, X is a multi-channel signal that contains all concatenated epochs from 1 to N and Y is a signal that contains N times the average over all epochs concatenated (with N being the number of all epochs from one participant's recording); in other words, $\underline{Y}$ is the same size as X, only that instead of single trials (as in the case of X) it is made up of repetitions of the average of all trials, again using the same latency range as in X. More precisely, both X and Y are of size [number of channels × number of samples] and both w_x and w_y are of size [number of channels × number of channels] (in the case

of full rank), with "number of channels" being 64 for EEG and 17 for ESG and "number of samples" being N (2000 in case of no trial rejection) * 11 (see below for rationale). Applied in this way, the CCA procedure serves as a template matching between the single-trial and the average of all trials. The spatial filter w_x corresponds to a spatial weighting of the multi-channel signal to separate SEP-related activity from background noise [42]. Since we were interested in early components of the SEP, we only subjected a short time window to CCA (and not the whole epoch length), namely a window from 5 ms before to 5ms after the peak of the cortical or spinal SEP component of interest (resulting in 11 data points per trial). The extracted spatial filter was then applied to the whole length of the epochs. To compute the spatial activity pattern of each CCA component, the spatial filters w_x were multiplied by the covariance matrix of X in order to take the data's noise structure into account [118]. For each stimulation (median or tibial nerve stimulation), one CCA component was selected for further analyses. These components differed in the different data sets and in the different stimulation conditions: in EEG data of median nerve stimulation, the spatial pattern of the selected CCA component corresponded to the typical N20-P35 tangential dipole over the central sulcus and in EEG data of tibial nerve stimulation, it corresponded to the typical P40 radial dipole over medial somatosensory areas. In ESG data of median nerve stimulation, the spatial pattern of the selected CCA component corresponded to a radial dipole (ventral-dorsal direction) over cervical areas as typical for N13 and in ESG data of tibial nerve stimulation it corresponded to a radial dipole over lumbar areas of the spinal cord as typical for the N22. As expected, the selected component was present in all participants among the first two CCA components, i.e., those with the largest canonical correlation coefficients: for spinal data, we selected the first component in every participant (median first component: N = 36; tibial first component: N = 36) and for cortical data, we nearly always selected the first component (median first component: N = 32; median second component: N = 4; tibial first component: N = 35; tibial second component: N = 1). Because CCA is not sensitive to the polarity of the signal, the spatial filters were multiplied by -1 if necessary, so that the extracted SEP component of interest would always result in the expected peak direction (negative for the cortical N20 and the spinal N13 in the mixed-hand condition, positive for the cortical P40 and negative for the spinal N22 in the mixed-foot condition). Note that for EEG, all channels were subjected to CCA, while for ESG only channels from the electrode patch of interest were subjected to CCA (i.e., the cervical patch in the hand-mixed condition and the lumbar patch in the foot-mixed condition). Last but not least, it is important to note that for such a multivariate analysis the number of samples should in principle be at least ten times the number of variables [119], though more recent efforts also taking into account the effect size suggest an even larger sample-to-feature ratio: e.g. in the case of a between-set correlation of 0.3 (close to the average canonical correlations we observed: 0.25 for median and 0.29 for tibial nerve stimulation) at least 50 samples per feature [120]. In our case, we far exceed the suggested sample-to-feature ratio due to very large number of trials used for training (i.e. in the case of no trial rejections, 2000 trials with 11 data points each compared to 64 (EEG) or 17 (ESG) channels).

Brainstem potentials. Cleaned and epoched EEG and ESG signals, which had been re-referenced during preprocessing to Fz, were combined into one dataset and referenced to a common reference at FPz, since frontal channels have been suggested for the investigation of brainstem potentials [27,121,122]. The N14 brainstem potential following median nerve stimulation was extracted from channel SC1 and the N30 brainstem potentials following tibial nerve stimulation was extracted from channel S3 (these potentials have also been described as P14 and P30 in the literature, when using FPz as the active electrode). Please note that we also aimed to apply CCA to brainstem potentials as well, but did not succeed.

Potential amplitude and latency. For each participant, NAP and SEP latencies were defined individually at the peak of the potential in the average trace over all trials. At the cortical level, SEP latency and amplitude were determined in the CCA component [40–42]. At the spinal level, SEP latency was determined in anatomically-defined channels (SC6 for cervical and L1 for lumbar

potentials, both thoracic (TH6) referenced) and in the CCA component. Spinal amplitudes were determined in the same channels with thoracic or anterior reference as well as in the cervical or lumbar CCA component. Note that all average traces were visually inspected. In case one of the potentials was not visible in a participant, its latency was estimated based on the average latency of that potential over all participants and the amplitude was extracted at the estimated latency (Table 1 shows in the column "#" the number of participants in which potentials were detected at the individual level).

Statistical analysis. First, to statistically characterize the response in well-known early potentials, we tested peripheral NAP and early SEP peak-amplitudes against zero using one-sample t-tests. Second, we investigated whether we might also observe possible later-occurring potentials. For this analysis, we followed the same preprocessing steps, but now filtered with a broader frequency band (5 Hz to 400 Hz), since later components could have lower frequency content. Using resting-state data from the same participants obtained at the very beginning of Experiment 1, we created a surrogate time series with the same stimulation sequence that we preprocessed in the same way. Over a region of interest consisting of the three central columns of the cervical or lumbar electrode grid, we systematically compared the signal from stimulation-runs and from rest-runs in the time window from 0 ms (stimulation onset) to 600 ms using a cluster-based permutation test (in space and time using the FieldTrip toolbox [123]) and focused on responses occurring after the above-reported early potentials (the cluster-based permutation test also identified the N13 and N22, but these are ignored here). In all analyses, significance was established at $p < 0.05$.

Time-frequency analysis. For each participant, time-frequency analysis was performed on the averaged trial signal using a continuous short-time fast Fourier transform with a window length of 21 ms and normalized to a baseline interval from 200 ms to 10 ms before stimulus onset. The average over all participants was then displayed.

Signal-to-noise ratio (SNR). For all potentials, the SNR was quantified as the root-mean-square of the signal (extracted in a in a time window of +/-1 ms around the individual peak latency) divided by the root-mean-square of the noise (extracted in the same time window before the stimulus onset).

Assessing the robustness of spinal SEPs. In order to aid in the planning of future experiments, we assessed the robustness of spinal SEPs as a function of trial number and sample size. Towards this end, we extracted single-trial SEP amplitudes from each participant at the peak latency identified in the average over all trials of that participant, both from anatomically-defined channels (with reference at TH6) and from CCA components (trained on the entire data).

Based on these data, we carried out two analyses. *First*, we assessed the minimum number of trials to obtain a significant result at the level of a *single participant*. For each participant, a subset of trials (trial number varying between 5 and 1000 in steps of 10, including 1000) was sampled with replacement and the significance of amplitudes in the sampled trials was determined using a one-sample t-test ($p < 0.05$). This procedure was repeated 1000 times for each participant and we report the proportion of significant results for each participant. *Second*, we determined the minimum number of trials and participants to obtain a significant *group-level* effect. Therefore, we employed Monte Carlo analyses and simulated a large number of experiments[124]. For each 'experiment', first, a subset of participants (number varying between 5, 10, 15, 20, 25, 30, 35, 36) was sampled with replacement and then a subset of trials (number varying between 5 to 1000 in steps of 10, including 1000) was sampled with replacement. The trials were then averaged and a one-sample t-test was used to determine the significance. Each experiment was repeated 1000 times and we report the proportion of experiments that yielded a significant result (at $p < 0.05$). It is important to note that CCA was only trained once on all trials of mixed-nerve data and then spatial filters were applied to the relevant data, as re-running CCA for each "experiment" was not feasible computationally.

Data processing and statistical analysis (Experiment 2)

Data processing and analyses followed what is described above for Experiment 1, except that in addition to the hand-mixed and foot-mixed conditions, there were also the hand-sensory (finger1, finger2, fingers1&2) and foot-sensory (toe1, toe2, toes1&2) conditions.

Stimulation artifact removal. Identical to Experiment 1, we defined individual artifact windows in cervical and lumbar ESG channels. At the cervical level, average artifact windows ranged from -2.0 ms (std = 1.1 ms) to 4.2 ms (std = 1.8 ms) and at the lumbar level from -2.0 ms (std = 1.1 ms) to 4.8 ms (std = 2.0 ms).

EEG data preprocessing. EEG preprocessing was performed in the same way as described above for Experiment 1. One noisy channel was identified in each of 6 participants and interpolated before ICA. One difference to the EEG analysis described in Experiment 1 was that in step three the ICs identified as representing artifactual sources were removed from the EEG signal that i) consisted of concatenated blocks of each stimulation condition only (i.e., hand-mixed, foot-mixed, hand sensory, or foot-sensory) and ii) had zero-phase IIR filtering applied with a 50-Hz comb filter (40th order, bandwidth 0.003) and a band-pass (30-400 Hz) Butterworth filter (4th order); the change in filtering was due to additional line noise and its harmonics introduced by electrical stimulation via ring electrodes. Identical to Experiment 1, noisy time points were removed, but here this did not result in the exclusion of additional channels. In Experiment 2, epochs were cut from 200 ms before to 300 ms after stimulus onset and baseline-corrected (with a reference interval from -110 ms to -10 ms before stimulus onset). Across conditions, this procedure resulted in the following number of trials remaining on average: hand-sensory 99.5% (range across participants: 5795 trials to 6000 trials), hand-mixed 99.4% (range across participants: 1921 trials to 2000 trials), foot-sensory 99.2% (range across participants: 5678 trials to 6000 trials), and foot-mixed 99.8% (range across participants: 1978 trials to 2000 trials).

ESG data preprocessing. Since ESG data were preprocessed the same way as described in Experiment 1, only the differences are listed in the following. After cardiac artifact correction, an average of 1.8 channels (std = 1.0) were removed in four participants. Due to the use of ring electrodes for digit stimulation, more line noise and its harmonics were visible in the data. Therefore, zero-phase IIR filtering was applied with a 50-Hz comb filter (40th order, bandwidth 0.003) and a band-pass (30-400 Hz) Butterworth filter (4th order). Similar to Experiment 1, time points with ESG activity above 100 µV were removed from the continuous data, and if more than 50% of data points were removed from a channel, the whole channel was excluded instead. In one participant, two additional channels were removed. The signal was cut into epochs with the same time range as reported for the EEG signal (from -200 ms to to 300 ms around stimulus onset) and epochs were baseline-corrected (reference window -110 ms to -10 ms before stimulus onset). On average, 91.3% of trials remained in the hand-mixed condition (range across participants: 999 trials to 2000 trials), 90.5% of trials remained in the hand-sensory conditions (range across participants: 3873 trials to 5993 trials), 94.2% of trials remained in the foot-mixed condition (range across participants: 1433 trials to 2000 trials), and 91.4% of trials remained in the foot-sensory conditions (range across participants: 3751 trials to 5988 trials).

ENG data preprocessing. ENG data were processed the same way as described for Experiment 1 above.

CCA. CCA was trained in the same way as explained above for Experiment 1. More specifically, it was trained on data from mixed nerve conditions (due to their higher SNR) and the spatial filters were then applied to the respective mixed and sensory nerve conditions. The selected component was present in all participants among the first two CCA components, i.e., those with the largest canonical correlation coefficients: for spinal data, we selected the first component in every participant (median first component: N = 24; tibial first component: N = 24) and for cortical data,

we nearly always selected the first component (median first component: N = 20; median second component: N = 4; tibial first component: N = 22; tibial second component: N = 2).

Brainstem potentials. We did not investigate brainstem potentials in Experiment 2 due to the lower SNR of SEPs after sensory nerve stimulation.

Potential amplitude and latency. These metrics were calculated in identical fashion as described for Experiment 1.

Statistical analysis. SEP amplitudes from all experimental conditions were compared against zero using one-sample t-tests. SEP amplitudes and latencies in mixed and sensory conditions were compared using paired t-tests. To balance the number of stimuli for mixed and sensory conditions only the double stimulation conditions were subjected to this statistical comparison.

Signal-to-noise ratio (SNR). For all potentials, the SNR was quantified as the root-mean-square of the signal (extracted in a in a time window of +/-1 ms around the individual peak latency) divided by the root-mean-square of the noise (extracted in the same time window before the stimulus onset).

Assessing the robustness of spinal SEPs. In order to also assess the robustness of the spinal SEPs elicited by sensory nerve stimulation, we repeated the same analyses as outlined for Experiment 1, though this time for the conditions finger1, finger2, fingers1&2, toe1, toe2, and toes1&2). Please note that we adjusted the number of participants (number varying between 5, 10, 15, 20, 24) according to the smaller sample size of Experiment 2.

Linear-mixed-effects models across somatosensory processing levels. To examine whether electrophysiological signals covaried across different stages of somatosensory processing, we employed linear-mixed-effects (LME) models. Specifically, we tested whether the effect of stimulation condition (mixed nerve, finger/toe1, finger/toe2, fingers/toes1&2) on signal amplitude propagated through the somatosensory processing hierarchy. For this, we used random-intercept LME models with the random factor subject, and in- or excluding the factor stimulation condition (with mixed nerve as reference level) to the regressions of peak amplitudes on consecutive somatosensory processing levels in the following way:

$$spinal\ cord \sim 1 + periphery + (1 \mid subject)$$

$$spinal\ cord \sim 1 + periphery * condition + (1 \mid subject)$$

$$S1 \sim 1 + spinal\ cord + (1 \mid subject)$$

$$S1 \sim 1 + spinal\ cord * condition + (1 \mid subject).$$

These analyses were separately performed for stimulation conditions of the hand and the foot. Variables ‘spinal cord’ and ‘S1’ correspond to the single-trial peak amplitudes of the respective signals extracted using CCA as explained in the methods section “2.6.5: CCA”, and ‘periphery’ to the peripheral single-trial NAP peak amplitude measured at the axilla or popliteal fossa in hand and foot stimulation, respectively (in foot stimulation, the signal was derived from the knee electrode with the largest evoked potential). All amplitude measures were z-transformed before including them in the LME models. The fixed-effect coefficients were estimated based on the maximum likelihood (ML) and p values of the fixed-effect coefficients were obtained adjusting the denominator degrees of freedom according to Satterthwaite’s method [125]. The LME models were calculated in R (version 4.2.0 [126]) with the lmer function of the lme4 package (version 1.1-30 [127]), as well as including the lmerTest package (version 3.1-3 [128]) for the implementation of the Satterthwaite method.

Interaction ratio. If the information from the simultaneous stimulation of two digits (fingers or toes) is integrated at a certain neural processing stage, then the SEP amplitude following this simultaneous digit stimulation should be reduced compared to arithmetic sum of the SEP amplitudes following separate stimulation of the two digits. To quantify this attenuation effect for each participant, we calculated an interaction ratio (IR) as suggested previously [44,45,129]. The IR captures the amplitude attenuation caused by the simultaneous stimulation of two digits and describes this attenuation as percentage of the expected amplitude sum of single-digit stimulations:

$$IR = (\sum(D1,D2) - D1D2) / \sum(D1,D2) * 100$$

where ∑(D1,D2) is the sum over SEP (or NAP) amplitudes following single-digit (finger/toe1 or finger/toe2) stimulation and D1D2 the SEP (or NAP) amplitude following double-digit stimulation (fingers/toes1&2). A positive IR would reflect the percentage of SEP amplitude attenuation from the expected amplitude (i.e., the sum of SEP amplitudes to single-digit stimulation) and an IR of 0% would suggest that there is no integration happening, meaning SEP amplitudes to double-digit and the sum of single-digit stimulations have the same size (a negative IR would mean that there is an amplification effect of SEP amplitudes to double-digit stimulation). IR values from each participant to finger and toe stimulation were tested against zero using one-sample t-tests.

Experiment 3: nociceptive stimulation

Participants. We acquired data from seven healthy volunteers (5 female; mean age: 30.6 years, range: 23-36 years), all of whom provided written informed consent. The study was approved by the Ethics Committee at the Medical Faculty of the University of Leipzig

Laser stimulation. Individually calibrated painful heat stimuli (duration 125ms) were delivered to the dorsum of left hand using a CO_2-laser with a with a wavelength of 10.6µm and a beam diameter of 6mm (LSD; Laser Stimulation Device, SIFEC s.a., Ferrières, Belgium). The LSD contains a closed loop temperature control system to maintain constant skin temperature during stimulation by adjusting the energy output. The stimulus position was controlled by an electric motor moving the laser head relative to a participant's hand, allowing for precise control of stimulation position. Throughout the entire experiment, participants wore protective goggles.

Experimental design. The here-reported data are part of a larger experiment also involving other stimulation modalities, but we solely focus on laser stimulation in this report. Before any electrodes were attached to the participant, the experiment started with a calibration procedure in order to find temperatures that would be perceived as clearly painful, but tolerable (mean temperature: 55.9°C; range: 53-59°C). There were 10 blocks of laser stimulation (with a break of ~5-10 minutes between blocks), with each block containing 36 stimuli, separated by an ISI of 1.53s with a jitter between +/-100ms (drawn from a uniform distribution). In each block, the laser beam was shifted over the dorsum of the left hand in an S-shaped pattern along a 6x6 grid (size 5x5cm): the start could be in any of the 4 corners of the grid and the laser would always move along the rows in the anterior/posterior direction before moving to the next column, until all 36 cells had been stimulated once.

Electrographic recordings. ECG, EEG, EOG, and ESG data were acquired using the same equipment as described in Experiment 1 and Experiment 2. ECG data were recorded via an electrode placed on the left costal arch, referenced to an electrode placed underneath the right clavicular. EEG data were recorded via a standard 32-channel montage according to the 10-20 system and referenced to the nose. EOG data were recorded via two additional electrodes placed on the canthus of the right eye (referenced to nose) and below the right eye (referenced to Fp2). ESG recordings were again based on a custom-made electrode patch (consisting of the same fabric as the EEG cap), but now with a higher electrode number than in Experiment 1 and Experiment 2

and focused solely on the cervical spinal cord. The patch consisted of 38 electrodes centred around an electrode over the spinous process of the 7th cervical vertebra. The midline of this electrode-grid was positioned vertically along the spine and consisted of 7 electrodes (the 4th one being centered on vertebra C7) with a vertical inter-electrode distance of 2 cm. Two further vertical lines of 6 electrodes each were placed 1.5 cm to the right and left of the midline electrodes, another two vertical lines of 5 electrodes were placed 3 cm to the right and left of the midline, and another two vertical lines of 2 electrodes each were placed 5 cm to the right and left of the midline. Additional electrodes were placed on the 1st cervical vertebra and on the inion. In addition to the dorsal electrodes, there were also 3 ventral electrodes at the anterior neck (one supra-glottic electrode (CA1), one above the suprasternal notch (CA3) and the third one in the middle between these two (CA2)). ESG data were referenced to an electrode positioned over the spinous process of the 6th thoracic vertebra (Th6). The active ground electrode stabilized the signal via the "driven right leg" principle. It was placed at POz in the EEG montage and on the spinous process of the 10th thoracic vertebra in the ESG montage.

Data analysis – EEG. All analyses were performed using Python 3.10 and MNE (https://mne.tools/stable/index.html; version 1.6.0). Data from the 10 experimental blocks were concatenated and down-sampled to 500Hz. Down-sampled data were then high-pass filtered at 1 Hz (using a 4th order Butterworth filter, effective order 8) and notch filtered around 50Hz and harmonics (using an 8th order Butterworth filter, effective order 16). Subsequently, data were epoched in a window between 300ms before and 1000ms after stimulus onset. Invalid trials (i.e. aborts of the laser) were removed, followed by a manual removal of extremely noisy epochs as determined by visual inspection. Data was further low-pass filtered with a cutoff frequency of 30Hz (4th order Butterworth filter) and either re-referenced to the average of all EEG electrodes (for analysis of the N2P2 complex) or to Fz (for analysis of the N1).

Data analysis – ESG. All analyses were performed using Python 3.10 and MNE (https://mne.tools/stable/index.html; version 1.6.0). First, in order to remove possible artefacts resulting from stimulation, data were linearly interpolated between -13ms and 13ms relative to stimulus onset. Data were then down sampled to 1kHz, and notch filtered to remove powerline noise at 50Hz and all harmonics up to 200Hz with an IIR filter. Next, the cardiac artefact was removed using signal space projection with 6 projectors and the data were bandpass filtered from 30Hz to 150Hz using a 4th order Butterworth, zero-phase filter. The data were then epoched from –100ms to 300ms relative to stimulation, with the baseline period defined from –100ms to –10ms. Finally, CCA was applied as described previously for Experiment 1 and Experiment 2, with the onset and duration of the training window changed based on the following reasoning.

Surface recordings show that with appropriate task / analysis, one can observe laser-evoked cortical responses peaking as soon as 83ms (EEG data; [130]) or 98ms (MEG-data; onset at 84ms; [131]) after stimulation onset, with invasive recordings revealing that the onset of cortical responses to laser stimulation can be early as ~70ms in S1 [132]. Invasive thalamic recordings demonstrate spikes between 60 and 70ms [133] and induced responses in the gamma range at ~90ms [134] after laser stimulation (but see [135] for later responses). fMRI-EEG fusion results points towards thalamic responses to laser stimulation from 65ms (in a lateral nucleus) and 89ms (in a medial nucleus) onwards [136]. Together, these evoked-response data suggest that initial spinal responses could occur even before 60ms. With respect to conduction-velocity data, estimates of human spinothalamic tract conduction velocity vary between laboratories and employed methods (see [137] and responses by Rossi et al. and Kagiki) and have been shown to differ in various spinothalamic pathways [138–140]. We thus did not base our estimation as to when expect spinal responses on these estimates, but instead additionally relied on peripheral nerve conduction velocity estimates of A-delta fibres mediating responses to laser stimulation. These have been estimated to vary between 9-18m/s ([141]: 9m/s; [142]: 11m/s; [143]: 13m/s; [144]: 16m/s; [133]: 18m/s) and

thus suggest possible initial spinal responses to occur roughly 45ms to 90ms after stimulation when i) considering an approximate distance of 80cm between hand dorsum and spinal cord and ii) ignoring any delay between laser stimulation onset and action potential generation in the peripheral nerve. Based on the above considerations, we trained CCA on a time-window of 45ms to 90ms after laser stimulation onset - this is only a heuristic for this first proof-of-principle experiment and it is likely that future studies investigating electrophysiological spinal responses in much more detail might lead to more optimized training windows.

For each participant, the first CCA component (as ranked by their canonical correlation coefficient) was selected and the resulting time-courses were averaged across participants to obtain a group-average response. Since CCA is not sensitive to the polarity of the signal and since we observed a negative deflection at ~50ms in the component time-course in 6 out of 7 participants (but a positive deflection at this time-point in participant 2), we multiplied this participant's time-course by -1 and used this sign-inverted time-course in all further analyses (similar to the procedure used in Experiment 1 and Experiment 2). In order to demonstrate the robustness of the obtained results, we also performed a within-participant four-fold split of the data (i.e. first split: trials 1,5,9,…; second split: trials 2,6,10,…; third split: trials 3,7,11,…; fourth split(trials: 4,8,12,…) after having applied the spatial filter and then averaged the results of each fold across participants.

Open science

Experiment 1 and Experiment 2 were preregistered on the Open Science Framework before the start of data acquisition and the preregistrations are openly available (see https://osf.io/sgptz and https://osf.io/mjdha); differences between the analyses suggested in the preregistrations and the analyses carried out here are listed in the Supplementary Material. All data are openly available (https://openneuro.org/datasets/ds004388, https://openneuro.org/datasets/ds004389, https://openneuro.org/datasets/ds005307) in EEG-BIDS format [145,146]. All analysis code has been deposited on GitHub and is openly available (see https://github.com/eippertlab/spinal_sep1, https://doi.org/10.5281/zenodo.13383050; https://github.com/eippertlab/spinal_sep2, https://doi.org/10.5281/zenodo.13383046; https://github.com/eippertlab/spinal-lep1, https://doi.org/10.5281/zenodo.13383056).

Acknowledgments

We would like to thank our student research assistants Janek Haschke, Pia-Lena Baisch, Paula Kosel, Max Braune, Samuel Simeon, and Marleen Löffler for their help in recruitment and data acquisition.

Funding

FE received funding from the Max Planck Society and the European Research Council (under the European Union's Horizon 2020 research and innovation programme; grant agreement No 758974).

Data and materials availability

All data, code, and materials used in the analyses are available as indicated above in the section "Open science".

Competing interests

The authors declare that they have no competing interests

References

1. Hochman S. Spinal cord. Curr Biol CB. 2007;17: R950-955. doi:10.1016/j.cub.2007.10.014

2. Abraira VE, Kuehn ED, Chirila AM, Springel MW, Toliver AA, Zimmerman AL, et al. The Cellular and Synaptic Architecture of the Mechanosensory Dorsal Horn. Cell. 2017;168: 295-310.e19. doi:10.1016/j.cell.2016.12.010

3. Chirila AM, Rankin G, Tseng S-Y, Emanuel AJ, Chavez-Martinez CL, Zhang D, et al. Mechanoreceptor signal convergence and transformation in the dorsal horn flexibly shape a diversity of outputs to the brain. Cell. 2022;185: 4541-4559.e23. doi:10.1016/j.cell.2022.10.012

4. Häring M, Zeisel A, Hochgerner H, Rinwa P, Jakobsson JET, Lönnerberg P, et al. Neuronal atlas of the dorsal horn defines its architecture and links sensory input to transcriptional cell types. Nat Neurosci. 2018;21: 869–880. doi:10.1038/s41593-018-0141-1

5. Ahuja CS, Wilson JR, Nori S, Kotter MRN, Druschel C, Curt A, et al. Traumatic spinal cord injury. Nat Rev Dis Primer. 2017;3: 17018. doi:10.1038/nrdp.2017.18

6. Ciccarelli O, Cohen JA, Reingold SC, Weinshenker BG, International Conference on Spinal Cord Involvement and Imaging in Multiple Sclerosis and Neuromyelitis Optica Spectrum Disorders. Spinal cord involvement in multiple sclerosis and neuromyelitis optica spectrum disorders. Lancet Neurol. 2019;18: 185–197. doi:10.1016/S1474-4422(18)30460-5

7. Colloca L, Ludman T, Bouhassira D, Baron R, Dickenson AH, Yarnitsky D, et al. Neuropathic pain. Nat Rev Dis Primer. 2017;3: 17002. doi:10.1038/nrdp.2017.2

8. Kathe C, Skinnider MA, Hutson TH, Regazzi N, Gautier M, Demesmaeker R, et al. The neurons that restore walking after paralysis. Nature. 2022;611: 540–547. doi:10.1038/s41586-022-05385-7

9. Rowald A, Komi S, Demesmaeker R, Baaklini E, Hernandez-Charpak SD, Paoles E, et al. Activity-dependent spinal cord neuromodulation rapidly restores trunk and leg motor functions after complete paralysis. Nat Med. 2022;28: 260–271. doi:10.1038/s41591-021-01663-5

10. Leone C, Di Stefano G, Di Pietro G, Bloms-Funke P, Boesl I, Caspani O, et al. IMI2-PainCare-BioPain-RCT2 protocol: a randomized, double-blind, placebo-controlled, crossover, multicenter trial in healthy subjects to investigate the effects of lacosamide, pregabalin, and tapentadol on biomarkers of pain processing observed by non-invasive neurophysiological measurements of human spinal cord and brainstem activity. Trials. 2022;23: 739. doi:10.1186/s13063-022-06431-5

11. Tracey I, Woolf CJ, Andrews NA. Composite Pain Biomarker Signatures for Objective Assessment and Effective Treatment. Neuron. 2019;101: 783–800. doi:10.1016/j.neuron.2019.02.019

12. Shekhtmeyster P, Carey EM, Duarte D, Ngo A, Gao G, Nelson NA, et al. Multiplex translaminar imaging in the spinal cord of behaving mice. Nat Commun. 2023;14: 1427. doi:10.1038/s41467-023-36959-2

13. Shekhtmeyster P, Duarte D, Carey EM, Ngo A, Gao G, Olmstead JA, et al. Trans-segmental imaging in the spinal cord of behaving mice. Nat Biotechnol. 2023. doi:10.1038/s41587-023-01700-3

14. Sandrini G, Serrao M, Rossi P, Romaniello A, Cruccu G, Willer JC. The lower limb flexion reflex in humans. Prog Neurobiol. 2005;77: 353–395. doi:10.1016/j.pneurobio.2005.11.003

15. Schieppati M. The Hoffmann reflex: a means of assessing spinal reflex excitability and its descending control in man. Prog Neurobiol. 1987;28: 345–376. doi:10.1016/0301-0082(87)90007-

16. Yoshizawa T, Nose T, Moore GJ, Sillerud LO. Functional magnetic resonance imaging of motor activation in the human cervical spinal cord. NeuroImage. 1996;4: 174–182. doi:10.1006/nimg.1996.0068

17. Cohen-Adad J. Functional Magnetic Resonance Imaging of the Spinal Cord: Current Status and Future Developments. Semin Ultrasound CT MR. 2017;38: 176–186. doi:10.1053/j.sult.2016.07.007

18. Curio G, Erné SN, Sandfort J, Scheer J, Stehr R, Trahms L. Exploratory mapping of evoked neuromagnetic activity from human peripheral nerve, brachial plexus and spinal cord. Electroencephalogr Clin Neurophysiol. 1991;81: 450–453.

19. Sumiya S, Kawabata S, Hoshino Y, Adachi Y, Sekihara K, Tomizawa S, et al. Magnetospinography visualizes electrophysiological activity in the cervical spinal cord. Sci Rep. 2017;7: 2192. doi:10.1038/s41598-017-02406-8

20. Cracco RQ. The initial positive potential of the human scalp-recorded somatosensory evoked response. Electroencephalogr Clin Neurophysiol. 1972;32: 623–629. doi:10.1016/0013-4694(72)90099-5

21. Cracco RQ. Spinal evoked response: peripheral nerve stimulation in man. Electroencephalogr Clin Neurophysiol. 1973;35: 379–386. doi:10.1016/0013-4694(73)90195-8

22. Jones SJ. Short latency potentials recorded from the neck and scalp following median nerve stimulation in man. Electroencephalogr Clin Neurophysiol. 1977;43: 853–863. doi:10.1016/0013-4694(77)90008-6

23. Liberson WT, Gratzer M, Zalis A, Grabinski B. Comparison of conduction velocities of motor and sensory fibers determined by different methods. Arch Phys Med Rehabil. 1966;47: 17–23.

24. Matthews WB, Beauchamp M, Small DG. Cervical somato-sensory evoked responses in man. Nature. 1974;252: 230–232. doi:10.1038/252230a0

25. Delbeke J, McComas AJ, Kopec SJ. Analysis of evoked lumbosacral potentials in man. J Neurol Neurosurg Psychiatry. 1978;41: 293–302. doi:10.1136/jnnp.41.4.293

26. Desmedt JE, Cheron G. Prevertebral (oesophageal) recording of subcortical somatosensory evoked potentials in man: the spinal P13 component and the dual nature of the spinal generators. Electroencephalogr Clin Neurophysiol. 1981;52: 257–275.

27. Desmedt JE, Huy NT. BIT-mapped colour imaging of the potential fields of propagated and segmental subcortical components of somatosensory evoked potentials in man. Electroencephalogr Clin Neurophysiol. 1984;58: 481–497. doi:10.1016/0013-4694(84)90037-3

28. Emerson RG, Seyal M, Pedley TA. Somatosensory evoked potentials following median nerve stimulation. I. The cervical components. Brain J Neurol. 1984;107 (Pt 1): 169–182.

29. Ratto S, Abbruzzese M, Abbruzzese G, Favale E. Surface recording of the spinal ventral root discharge in man. An experimental study. Brain J Neurol. 1983;106 (Pt 4): 897–909. doi:10.1093/brain/106.4.897

30. Yamada T, Kimura J, Nitz DM. Short latency somatosensory evoked potentials following median nerve stimulation in man. Electroencephalogr Clin Neurophysiol. 1980;48: 367–376. doi:10.1016/0013-4694(80)90129-7

31. Cruccu G, Aminoff MJ, Curio G, Guerit JM, Kakigi R, Mauguiere F, et al.

Recommendations for the clinical use of somatosensory-evoked potentials. Clin Neurophysiol. 2008;119: 1705–1719. doi:10.1016/j.clinph.2008.03.016

32. Mauguière F. Anatomic origin of the cervical N13 potential evoked by upper extremity stimulation. J Clin Neurophysiol. 2000;17: 236–245. doi:10.1097/00004691-200005000-00002

33. Boehme R, Hauser S, Gerling GJ, Heilig M, Olausson H. Distinction of self-produced touch and social touch at cortical and spinal cord levels. Proc Natl Acad Sci U S A. 2019;116: 2290–2299. doi:10.1073/pnas.1816278116

34. Chander BS, Deliano M, Azañón E, Büntjen L, Stenner M-P. Non-invasive recording of high-frequency signals from the human spinal cord. NeuroImage. 2022;253: 119050. doi:10.1016/j.neuroimage.2022.119050

35. Di Lionardo A, Di Stefano G, Leone C, Di Pietro G, Sgro E, Malara E, et al. Modulation of the N13 component of the somatosensory evoked potentials in an experimental model of central sensitization in humans. Sci Rep. 2021;11: 20838. doi:10.1038/s41598-021-00313-7

36. Pietro GD, Stefano GD, Leone C, Lionardo AD, Sgrò E, Blockeel AJ, et al. The N13 spinal component of somatosensory evoked potentials is modulated by heterotopic noxious conditioning stimulation suggesting an involvement of spinal wide dynamic range neurons. Neurophysiol Clin Clin Neurophysiol. 2021;51: 517–523. doi:10.1016/j.neucli.2021.09.001

37. Fabbrini A, Guerra A, Giangrosso M, Manzo N, Leodori G, Pasqualetti P, et al. Transcranial alternating current stimulation modulates cortical processing of somatosensory information in a frequency- and time-specific manner. NeuroImage. 2022;254: 119119. doi:10.1016/j.neuroimage.2022.119119

38. Rocchi L, Suppa A, Leodori G, Celletti C, Camerota F, Rothwell J, et al. Plasticity Induced in the Human Spinal Cord by Focal Muscle Vibration. Front Neurol. 2018;9: 935. doi:10.3389/fneur.2018.00935

39. Parra LC, Spence CD, Gerson AD, Sajda P. Recipes for the linear analysis of EEG. NeuroImage. 2005;28: 326–341. doi:10.1016/j.neuroimage.2005.05.032

40. Fedele T, Scheer H-J, Burghoff M, Waterstraat G, Nikulin VV, Curio G. Distinction between added-energy and phase-resetting mechanisms in non-invasively detected somatosensory evoked responses. Annu Int Conf IEEE Eng Med Biol Soc IEEE Eng Med Biol Soc Annu Int Conf. 2013;2013: 1688–1691. doi:10.1109/EMBC.2013.6609843

41. Waterstraat G, Fedele T, Burghoff M, Scheer H-J, Curio G. Recording human cortical population spikes non-invasively--An EEG tutorial. J Neurosci Methods. 2015;250: 74–84. doi:10.1016/j.jneumeth.2014.08.013

42. Stephani T, Hodapp A, Jamshidi Idaji M, Villringer A, Nikulin VV. Neural excitability and sensory input determine intensity perception with opposing directions in initial cortical responses. eLife. 2021;10: e67838. doi:10.7554/eLife.67838

43. Hoechstetter K, Rupp A, Stancák A, Meinck HM, Stippich C, Berg P, et al. Interaction of tactile input in the human primary and secondary somatosensory cortex--a magnetoencephalographic study. NeuroImage. 2001;14: 759–767. doi:10.1006/nimg.2001.0855

44. Hsieh CL, Shima F, Tobimatsu S, Sun SJ, Kato M. The interaction of the somatosensory evoked potentials to simultaneous finger stimuli in the human central nervous system. A study using direct recordings. Electroencephalogr Clin Neurophysiol. 1995;96: 135–142. doi:10.1016/0168-5597(94)00251-9

45. Ruben J, Krause T, Taskin B, Blankenburg F, Moosmann M, Villringer A. Sub-area-specific

Suppressive Interaction in the BOLD responses to simultaneous finger stimulation in human primary somatosensory cortex: evidence for increasing rostral-to-caudal convergence. Cereb Cortex. 2006;16: 819–826. doi:10.1093/cercor/bhj025

46. Magladery JW, Porter WE, Park AM, Teasdall RD. Electrophysiological studies of nerve and reflex activity in normal man. IV. The two-neurone reflex and identification of certain action potentials from spinal roots and cord. Bull Johns Hopkins Hosp. 1951;88: 499–519.

47. Pratt H, Starr A, Amlie RN, Politoske D. Mechanically and electrically evoked somatosensory potentials in normal humans. Neurology. 1979;29: 1236–1244. doi:10.1212/wnl.29.9_part_1.1236

48. Pratt H, Starr A. Mechanically and electrically evoked somatosensory potentials in human: scalp and neck distributions of short latency components. Electroencephalogr Clin Neurophysiol. 1981;51: 138–147. doi:10.1016/0013-4694(81)90002-x

49. Corniani G, Saal HP. Tactile innervation densities across the whole body. J Neurophysiol. 2020;124: 1229–1240. doi:10.1152/jn.00313.2020

50. Jiang N, Wang L, Huang Z, Li G. Mapping Responses of Lumbar Paravertebral Muscles to Single-Pulse Cortical TMS Using High-Density Surface Electromyography. IEEE Trans Neural Syst Rehabil Eng Publ IEEE Eng Med Biol Soc. 2021;29: 831–840. doi:10.1109/TNSRE.2021.3076095

51. Akaza M, Kawabata S, Ozaki I, Miyano Y, Watanabe T, Adachi Y, et al. Noninvasive measurement of sensory action currents in the cervical cord by magnetospinography. Clin Neurophysiol. 2021;132: 382–391. doi:10.1016/j.clinph.2020.11.029

52. Ushio S, Hoshino Y, Kawabata S, Adachi Y, Sekihara K, Sumiya S, et al. Visualization of the electrical activity of the cauda equina using a magnetospinography system in healthy subjects. Clin Neurophysiol Off J Int Fed Clin Neurophysiol. 2019;130: 1–11. doi:10.1016/j.clinph.2018.11.001

53. Yamada T. Neuroanatomic substrates of lower extremity somatosensory evoked potentials. J Clin Neurophysiol. 2000;17: 269–279. doi:10.1097/00004691-200005000-00005

54. Beall JE, Applebaum AE, Foreman RD, Willis WD. Spinal cord potentials evoked by cutaneous afferents in the monkey. J Neurophysiol. 1977;40: 199–211. doi:10.1152/jn.1977.40.2.199

55. Willis WD, Weir MA, Skinner RD, Bryan RN. Differential distribution of spinal cord field potentials. Exp Brain Res. 1973;17: 169–176. doi:10.1007/BF00235026

56. Shimoji K. Origins and properties of spinal cord evoked potentials. Atlas Hum Spinal Cord Evoked Potentials. 1995; 1–25.

57. Giesler GJ, Nahin RL, Madsen AM. Postsynaptic dorsal column pathway of the rat. I. Anatomical studies. J Neurophysiol. 1984;51: 260–275. doi:10.1152/jn.1984.51.2.260

58. Turecek J, Lehnert BP, Ginty DD. The encoding of touch by somatotopically aligned dorsal column subdivisions. Nature. 2022;612: 310–315. doi:10.1038/s41586-022-05470-x

59. Brown A. Organization in the spinal cord. Springer-Verlag; 1981. Available: https://cir.nii.ac.jp/crid/1572261549748274688

60. Ertekin C. Studies on the human evoked electrospinogram. I. The origin of the segmental evoked potentials. Acta Neurol Scand. 1976;53: 3–20. doi:10.1111/j.1600-0404.1976.tb04321.x

61. Shimoji K, Kano T, Higashi H, Morioka T, Henschel EO. Evoked spinal electrograms

recorded from epidural space in man. J Appl Physiol. 1972;33: 468–471. doi:10.1152/jappl.1972.33.4.468

62. Mizutani Y, Kuriki S. Somatically evoked magnetic fields in the vicinity of the neck. IEEE Trans Biomed Eng. 1986;33: 5l0-6. doi:10.1109/TBME.1986.325738

63. Mardell LC, Spedden ME, O'Neill GC, Tierney TM, Timms RC, Zich C, et al. Concurrent spinal and brain imaging with optically pumped magnetometers. J Neurosci Methods. 2024;406: 110131. doi:10.1016/j.jneumeth.2024.110131

64. Liu Y, Latremoliere A, Li X, Zhang Z, Chen M, Wang X, et al. Touch and tactile neuropathic pain sensitivity are set by corticospinal projections. Nature. 2018;561: 547–550. doi:10.1038/s41586-018-0515-2

65. Yamada T, Machida M, Kimura J. Far-field somatosensory evoked potentials after stimulation of the tibial nerve. Neurology. 1982;32: 1151–1158. doi:10.1212/wnl.32.10.1151

66. Lopes da Silva F. EEG and MEG: relevance to neuroscience. Neuron. 2013;80: 1112–1128. doi:10.1016/j.neuron.2013.10.017

67. Michel CM, Murray MM. Towards the utilization of EEG as a brain imaging tool. NeuroImage. 2012;61: 371–385. doi:10.1016/j.neuroimage.2011.12.039

68. Blankertz B, Lemm S, Treder M, Haufe S, Müller K-R. Single-trial analysis and classification of ERP components--a tutorial. NeuroImage. 2011;56: 814–825. doi:10.1016/j.neuroimage.2010.06.048

69. Nikulin VV, Nolte G, Curio G. A novel method for reliable and fast extraction of neuronal EEG/MEG oscillations on the basis of spatio-spectral decomposition. NeuroImage. 2011;55: 1528–1535. doi:10.1016/j.neuroimage.2011.01.057

70. Stephani T, Waterstraat G, Haufe S, Curio G, Villringer A, Nikulin VV. Temporal Signatures of Criticality in Human Cortical Excitability as Probed by Early Somatosensory Responses. J Neurosci Off J Soc Neurosci. 2020;40: 6572–6583. doi:10.1523/JNEUROSCI.0241-20.2020

71. Stephani T, Nierula B, Villringer A, Eippert F, Nikulin VV. Cortical response variability is driven by local excitability changes with somatotopic organization. NeuroImage. 2022; 119687.

72. Cadotte DW, Cadotte A, Cohen-Adad J, Fleet D, Livne M, Wilson JR, et al. Characterizing the location of spinal and vertebral levels in the human cervical spinal cord. AJNR Am J Neuroradiol. 2015;36: 803–810. doi:10.3174/ajnr.A4192

73. Reimann AF, Anson BJ. Vertebral level of termination of the spinal cord with report of a case of sacral cord. Anat Rec. 1944;88: 127–138. doi:10.1002/ar.1090880108

74. Severens M, Farquhar J, Desain P, Duysens J, Gielen C. Transient and steady-state responses to mechanical stimulation of different fingers reveal interactions based on lateral inhibition. Clin Neurophysiol Off J Int Fed Clin Neurophysiol. 2010;121: 2090–2096. doi:10.1016/j.clinph.2010.05.016

75. el-Negamy E, Sedgwick EM. Properties of a spinal somatosensory evoked potential recorded in man. J Neurol Neurosurg Psychiatry. 1978;41: 762–768. doi:10.1136/jnnp.41.8.762

76. Gandevia SC, Burke D, McKeon BB. Convergence in the somatosensory pathway between cutaneous afferents from the index and middle fingers in man. Exp Brain Res. 1983;50: 415–425. doi:10.1007/bf00239208

77. Tanosaki M, Suzuki A, Takino R, Kimura T, Iguchi Y, Kurobe Y, et al. Neural mechanisms

for generation of tactile interference effects on somatosensory evoked magnetic fields in humans. Clin Neurophysiol. 2002;113: 672–680. doi:10.1016/s1388-2457(02)00052-4

78. Le Bars D, Cadden SW. What is a wide-dynamic-range cell? Science of pain. Oxford, UK: Academic Press; 2009. pp. 331–338.

79. Plaghki L, Mouraux A. EEG and laser stimulation as tools for pain research. Curr Opin Investig Drugs Lond Engl 2000. 2005;6: 58–64.

80. Lejeune N, Petrossova E, Frahm KS, Mouraux A. High-speed heating of the skin using a contact thermode elicits brain responses comparable to CO2 laser-evoked potentials. Clin Neurophysiol Off J Int Fed Clin Neurophysiol. 2023;146: 1–9. doi:10.1016/j.clinph.2022.11.008

81. Iannetti GD, Baumgärtner U, Tracey I, Treede RD, Magerl W. Pinprick-evoked brain potentials: a novel tool to assess central sensitization of nociceptive pathways in humans. J Neurophysiol. 2013;110: 1107–1116. doi:10.1152/jn.00774.2012

82. Basbaum AI, Bautista DM, Scherrer G, Julius D. Cellular and molecular mechanisms of pain. Cell. 2009;139: 267–284. doi:10.1016/j.cell.2009.09.028

83. Heinricher MM, Tavares I, Leith JL, Lumb BM. Descending control of nociception: Specificity, recruitment and plasticity. Brain Res Rev. 2009;60: 214–225. doi:10.1016/j.brainresrev.2008.12.009

84. Kuner R. Spinal excitatory mechanisms of pathological pain. Pain. 2015;156 Suppl 1: S11-17. doi:10.1097/j.pain.0000000000000118

85. Niazy RK, Beckmann CF, Iannetti GD, Brady JM, Smith SM. Removal of FMRI environment artifacts from EEG data using optimal basis sets. NeuroImage. 2005;28: 720–737. doi:10.1016/j.neuroimage.2005.06.067

86. Chen WG, Schloesser D, Arensdorf AM, Simmons JM, Cui C, Valentino R, et al. The Emerging Science of Interoception: Sensing, Integrating, Interpreting, and Regulating Signals within the Self. Trends Neurosci. 2021;44: 3–16. doi:10.1016/j.tins.2020.10.007

87. Engelen T, Solcà M, Tallon-Baudry C. Interoceptive rhythms in the brain. Nat Neurosci. 2023;26: 1670–1684. doi:10.1038/s41593-023-01425-1

88. Barra B, Conti S, Perich MG, Zhuang K, Schiavone G, Fallegger F, et al. Epidural electrical stimulation of the cervical dorsal roots restores voluntary upper limb control in paralyzed monkeys. Nat Neurosci. 2022;25: 924–934. doi:10.1038/s41593-022-01106-5

89. Powell MP, Verma N, Sorensen E, Carranza E, Boos A, Fields DP, et al. Epidural stimulation of the cervical spinal cord for post-stroke upper-limb paresis. Nat Med. 2023;29: 689–699. doi:10.1038/s41591-022-02202-6

90. Davis KD, Aghaeepour N, Ahn AH, Angst MS, Borsook D, Brenton A, et al. Discovery and validation of biomarkers to aid the development of safe and effective pain therapeutics: challenges and opportunities. Nat Rev Neurol. 2020;16: 381–400. doi:10.1038/s41582-020-0362-2

91. Sluka KA, Wager TD, Sutherland SP, Labosky PA, Balach T, Bayman EO, et al. Predicting chronic postsurgical pain: current evidence and a novel program to develop predictive biomarker signatures. Pain. 2023;164: 1912–1926. doi:10.1097/j.pain.0000000000002938

92. Kuner R, Flor H. Structural plasticity and reorganisation in chronic pain. Nat Rev Neurosci. 2017;18: 20–30. doi:10.1038/nrn.2016.162

93. Prescott SA, Ma Q, De Koninck Y. Normal and abnormal coding of somatosensory stimuli causing pain. Nat Neurosci. 2014;17: 183–191. doi:10.1038/nn.3629

1618 94. D'Mello R, Dickenson AH. Spinal cord mechanisms of pain. Br J Anaesth. 2008;101: 8–
1619 16. doi:10.1093/bja/aen088

1620 95. Button KS, Ioannidis JPA, Mokrysz C, Nosek BA, Flint J, Robinson ESJ, et al. Power
1621 failure: why small sample size undermines the reliability of neuroscience. Nat Rev Neurosci.
1622 2013;14: 365–376. doi:10.1038/nrn3475

1623 96. McPherson JG, Bandres MF. Spontaneous neural synchrony links intrinsic spinal sensory
1624 and motor networks during unconsciousness. eLife. 2021;10: e66308. doi:10.7554/eLife.66308

1625 97. Ran C, Hoon MA, Chen X. The coding of cutaneous temperature in the spinal cord. Nat
1626 Neurosci. 2016. doi:10.1038/nn.4350

1627 98. Suzuki I, Mayanagi Y. Intracranial recording of short latency somatosensory evoked
1628 potentials in man: identification of origin of each component. Electroencephalogr Clin
1629 Neurophysiol. 1984;59: 286–296. doi:10.1016/0168-5597(84)90046-7

1630 99. Tinazzi M, Zanette G, Bonato C, Manganotti P, Polo A, Fiaschi A, et al. Neural generators
1631 of tibial nerve P30 somatosensory evoked potential studied in patients with a focal lesion of the
1632 cervicomedullary junction. Muscle Nerve. 1996;19: 1538–1548. doi:10.1002/(SICI)1097-
1633 4598(199612)19:12<1538::AID-MUS3>3.0.CO;2-B

1634 100. Boto E, Holmes N, Leggett J, Roberts G, Shah V, Meyer SS, et al. Moving
1635 magnetoencephalography towards real-world applications with a wearable system. Nature.
1636 2018;555: 657–661. doi:10.1038/nature26147

1637 101. Brookes MJ, Leggett J, Rea M, Hill RM, Holmes N, Boto E, et al. Magnetoencephalography
1638 with optically pumped magnetometers (OPM-MEG): the next generation of functional
1639 neuroimaging. Trends Neurosci. 2022;45: 621–634. doi:10.1016/j.tins.2022.05.008

1640 102. Vahdat S, Khatibi A, Lungu O, Finsterbusch J, Büchel C, Cohen-Adad J, et al. Resting-state
1641 brain and spinal cord networks in humans are functionally integrated. PLoS Biol. 2020;18:
1642 e3000789. doi:10.1371/journal.pbio.3000789

1643 103. Landelle C, Kinany N, Leener BD, Murphy ND, Lungu O, Marchand-Pauvert V, et al.
1644 Cerebro-spinal somatotopic organization uncovered through functional connectivity mapping.
1645 bioRxiv; 2024. p. 2024.04.11.588866. doi:10.1101/2024.04.11.588866

1646 104. Vahdat S, Lungu O, Cohen-Adad J, Marchand-Pauvert V, Benali H, Doyon J. Simultaneous
1647 Brain-Cervical Cord fMRI Reveals Intrinsic Spinal Cord Plasticity during Motor Sequence
1648 Learning. PLoS Biol. 2015;13: e1002186. doi:10.1371/journal.pbio.1002186

1649 105. Braaß H, Feldheim J, Chu Y, Tinnermann A, Finsterbusch J, Büchel C, et al. Association
1650 between activity in the ventral premotor cortex and spinal cord activation during force generation-
1651 A combined cortico-spinal fMRI study. Hum Brain Mapp. 2023;44: 6471–6483.
1652 doi:10.1002/hbm.26523

1653 106. Tinnermann A, Sprenger C, Büchel C. Opioid analgesia alters corticospinal coupling along
1654 the descending pain system in healthy participants. eLife. 2022;11: e74293.
1655 doi:10.7554/eLife.74293

1656 107. Oliva V, Hartley-Davies R, Moran R, Pickering AE, Brooks JC. Simultaneous brain,
1657 brainstem, and spinal cord pharmacological-fMRI reveals involvement of an endogenous opioid
1658 network in attentional analgesia. eLife. 2022;11: e71877. doi:10.7554/eLife.71877

1659 108. Spedden ME, O'Neill GC, Timms RC, West TO, Mellor S, Tierney TM, et al. Non-invasive
1660 evidence for rhythmic interactions between the human brain, spinal cord, and muscle. bioRxiv;
1661 2024. p. 2024.05.01.591590. doi:10.1101/2024.05.01.591590

109. Dykest RW, Terzis JK. Spinal nerve distributions in the upper Limb: The organization of the dermatome and afferent myotome. Philos Trans R Soc Lond B Biol Sci. 1981;293: 509–554. doi:10.1098/rstb.1981.0083

110. Lee MWL, McPhee RW, Stringer MD. An evidence-based approach to human dermatomes. Clin Anat N Y N. 2008;21: 363–373. doi:10.1002/ca.20636

111. Kwast-Rabben O, Libelius R, Heikkilä H. Somatosensory evoked potentials following stimulation of digital nerves. Muscle Nerve. 2002;26: 533–538. doi:10.1002/mus.10237

112. Desmedt JE, Cheron G. Spinal and far-field components of human somatosensory evoked potentials to posterior tibial nerve stimulation analysed with oesophageal derivations and non-cephalic reference recording. Electroencephalogr Clin Neurophysiol. 1983;56: 635–651.

113. Restuccia D, Di Lazzaro V, Valeriani M, Conti G, Tonali P, Mauguière F. Origin and distribution of P13 and P14 far-field potentials after median nerve stimulation. Scalp, nasopharyngeal and neck recording in healthy subjects and in patients with cervical and cervico-medullary lesions. Electroencephalogr Clin Neurophysiol Potentials Sect. 1995;96: 371–384. doi:10.1016/0168-5597(95)00054-V

114. Delorme A, Makeig S. EEGLAB: an open source toolbox for analysis of single-trial EEG dynamics including independent component analysis. J Neurosci Methods. 2004;134: 9–21. doi:10.1016/j.jneumeth.2003.10.009

115. Makeig S, Bell A, Jung T-P, Sejnowski TJ. Independent Component Analysis of Electroencephalographic Data. Advances in Neural Information Processing Systems. MIT Press; 1995.

116. De Clercq W, Vergult A, Vanrumste B, Van Paesschen W, Van Huffel S. Canonical correlation analysis applied to remove muscle artifacts from the electroencephalogram. IEEE Trans Biomed Eng. 2006;53: 2583–2587. doi:10.1109/TBME.2006.879459

117. Spüler M, Walter A, Rosenstiel W, Bogdan M. Spatial filtering based on canonical correlation analysis for classification of evoked or event-related potentials in EEG data. IEEE Trans Neural Syst Rehabil Eng Publ IEEE Eng Med Biol Soc. 2014;22: 1097–1103. doi:10.1109/TNSRE.2013.2290870

118. Haufe S, Meinecke F, Görgen K, Dähne S, Haynes J-D, Blankertz B, et al. On the interpretation of weight vectors of linear models in multivariate neuroimaging. NeuroImage. 2014;87: 96–110. doi:10.1016/j.neuroimage.2013.10.067

119. Mandeville GK, Roscoe JT. Fundamental Research Statistics for the Behavioral Sciences. 1971. Available: https://www.jstor.org/stable/2284880?origin=crossref

120. Helmer M, Warrington S, Mohammadi-Nejad A-R, Ji JL, Howell A, Rosand B, et al. On the stability of canonical correlation analysis and partial least squares with application to brain-behavior associations. Commun Biol. 2024;7: 217. doi:10.1038/s42003-024-05869-4

121. Tinazzi M, Zanette G, Polo A, Bonato C, Manganotti P, Fiaschi A, et al. Subcortical P30 potential following tibial nerve stimulation: detection and normative data. Ital J Neurol Sci. 1995;16: 623–628. doi:10.1007/BF02230912

122. Tinazzi M, Mauguière F. Assessment of intraspinal and intracranial conduction by P30 and P39 tibial nerve somatosensory evoked potentials in cervical cord, brainstem, and hemispheric lesions. J Clin Neurophysiol. 1995;12: 237–253. doi:10.1097/00004691-199505010-00003

123. Oostenveld R, Fries P, Maris E, Schoffelen J-M. FieldTrip: Open source software for advanced analysis of MEG, EEG, and invasive electrophysiological data. Comput Intell Neurosci.

2011;2011: 156869. doi:10.1155/2011/156869

124. Boudewyn MA, Luck SJ, Farrens JL, Kappenman ES. How many trials does it take to get a significant ERP effect? It depends. Psychophysiology. 2018;55: e13049. doi:10.1111/psyp.13049

125. Satterthwaite FE. An approximate distribution of estimates of variance components. Biometrics. 1946;2: 110–114.

126. R Core Team. R: A Language and Environment for Statistical Computing. Vienna: R Foundation for Statistical Computing; 2018.

127. Bates D, Mächler M, Bolker B, Walker S. Fitting Linear Mixed-Effects Models Using lme4. J Stat Softw. 2015;67: 1–48. doi:10.18637/jss.v067.i01

128. Kuznetsova A, Brockhoff PB, Christensen RHB. lmerTest Package: Tests in Linear Mixed Effects Models. J Stat Softw. 2017;82: 1–26. doi:10.18637/jss.v082.i13

129. Cataldo A, Ferrè ER, di Pellegrino G, Haggard P. Why the whole is more than the sum of its parts: Salience-driven overestimation in aggregated tactile sensations. Q J Exp Psychol 2006. 2019;72: 2509–2526. doi:10.1177/1747021819847131

130. Valeriani M, Restuccia D, Le Pera D, Fiaschetti L, Tonali P, Arendt-Nielsen L. Unmasking of an early laser evoked potential by a point localization task. Clin Neurophysiol Off J Int Fed Clin Neurophysiol. 2000;111: 1927–1933. doi:10.1016/s1388-2457(00)00439-9

131. Wang X, Inui K, Kakigi R. Early cortical activities evoked by noxious stimulation in humans. Exp Brain Res. 2007;180: 481–489. doi:10.1007/s00221-007-0878-3

132. Ohara S, Crone NE, Weiss N, Treede R-D, Lenz FA. Cutaneous painful laser stimuli evoke responses recorded directly from primary somatosensory cortex in awake humans. J Neurophysiol. 2004;91: 2734–2746. doi:10.1152/jn.00912.2003

133. Kobayashi K, Winberry J, Liu CC, Treede RD, Lenz FA. A painful cutaneous laser stimulus evokes responses from single neurons in the human thalamic principal somatic sensory nucleus ventral caudal (Vc). J Neurophysiol. 2009;101: 2210–2217. doi:10.1152/jn.91347.2008

134. Kim JH, Chien JH, Liu CC, Lenz FA. Painful cutaneous laser stimuli induce event-related gamma-band activity in the lateral thalamus of humans. J Neurophysiol. 2015;113: 1564–1573. doi:10.1152/jn.00778.2014

135. Bastuji H, Frot M, Mazza S, Perchet C, Magnin M, Garcia-Larrea L. Thalamic Responses to Nociceptive-Specific Input in Humans: Functional Dichotomies and Thalamo-Cortical Connectivity. Cereb Cortex. 2016;26: 2663–2676. doi:10.1093/cercor/bhv106

136. Tu Y, Li Z, Zhang L, Zhang H, Bi Y, Yue L, et al. Pain-preferential thalamocortical neural dynamics across species. Nat Hum Behav. 2024;8: 149–163. doi:10.1038/s41562-023-01714-6

137. Iannetti GD, Cruccu G, Manfredi M. The problem of conduction velocity of the human spinothalamic tract. Clin Neurophysiol Off J Int Fed Clin Neurophysiol. 2001;112: 1113–1116. doi:10.1016/s1388-2457(01)00493-x

138. Tsuji T, Inui K, Kojima S, Kakigi R. Multiple pathways for noxious information in the human spinal cord. Pain. 2006;123: 322–331. doi:10.1016/j.pain.2006.03.009

139. Valeriani M, Le Pera D, Restuccia D, de Armas L, Miliucci R, Betti V, et al. Parallel spinal pathways generate the middle-latency N1 and the late P2 components of the laser evoked potentials. Clin Neurophysiol Off J Int Fed Clin Neurophysiol. 2007;118: 1097–1104. doi:10.1016/j.clinph.2007.01.015

140. Treede R-D, Lenz FA. Passing lanes and slow lanes into the nociceptive network of the

human brain. Pain. 2006;123: 223–225. doi:10.1016/j.pain.2006.05.014

141. Kakigi R, Endo C, Neshige R, Kuroda Y, Shibasaki H. Estimation of conduction velocity of A delta fibers in humans. Muscle Nerve. 1991;14: 1193–1196. doi:10.1002/mus.880141209

142. Tran TD, Lam K, Hoshiyama M, Kakigi R. A new method for measuring the conduction velocities of Abeta-, Adelta- and C-fibers following electric and CO(2) laser stimulation in humans. Neurosci Lett. 2001;301: 187–190.

143. Obi T, Takatsu M, Yamazaki K, Kuroda R, Terada T, Mizoguchi K. Conduction velocities of Adelta-fibers and C-fibers in human peripheral nerves and spinal cord after CO2 laser stimulation. J Clin Neurophysiol Off Publ Am Electroencephalogr Soc. 2007;24: 294–297. doi:10.1097/WNP.0b013e318038f45f

144. Bromm B, Treede RD. Pain Related Cerebral Potentials: Late and Ultralate Components. Int J Neurosci. 1987;33: 15–23. doi:10.3109/00207458708985926

145. Gorgolewski KJ, Auer T, Calhoun VD, Craddock RC, Das S, Duff EP, et al. The brain imaging data structure, a format for organizing and describing outputs of neuroimaging experiments. Sci Data. 2016;3: 160044. doi:10.1038/sdata.2016.44

146. Pernet CR, Appelhoff S, Gorgolewski KJ, Flandin G, Phillips C, Delorme A, et al. EEG-BIDS, an extension to the brain imaging data structure for electroencephalography. Sci Data. 2019;6: 103. doi:10.1038/s41597-019-0104-8